



Early-Holocene warming in Beringia and its mediation by sea-level and vegetation changes

P. J. Bartlein¹, M. E. Edwards^{2,3}, S. W. Hostetler⁴, S. L. Shafer⁴, P. M. Anderson⁵, L. B. Brubaker⁶, and A. V. Lozhkin⁷

¹Department of Geography, University of Oregon, Eugene, Oregon, USA

²Geography and Environment, University of Southampton, Southampton, UK

³College of Natural Sciences and Mathematics, University of Alaska, Fairbanks, Alaska, USA

⁴U.S. Geological Survey, Corvallis, Oregon, USA

⁵Quaternary Research Center, University of Washington, Seattle, Washington, USA

⁶School of Environmental and Forest Sciences, University of Washington, Seattle, Washington, USA

⁷Northeast Interdisciplinary Research Institute, Far East Branch of the Russian Academy of Sciences, Magadan, Russia

Correspondence to: P. J. Bartlein (bartlein@uoregon.edu)

Received: 13 February 2015 – Published in Clim. Past Discuss.: 30 March 2015

Accepted: 18 August 2015 – Published: 24 September 2015

Abstract. Arctic land-cover changes induced by recent global climate change (e.g., expansion of woody vegetation into tundra and effects of permafrost degradation) are expected to generate further feedbacks to the climate system. Past changes can be used to assess our understanding of feedback mechanisms through a combination of process modeling and paleo-observations. The subcontinental region of Beringia (northeastern Siberia, Alaska, and northwestern Canada) was largely ice-free at the peak of deglacial warming and experienced both major vegetation change and loss of permafrost when many arctic regions were still ice covered. The evolution of Beringian climate at this time was largely driven by global features, such as the amplified seasonal cycle of Northern Hemisphere insolation and changes in global ice volume and atmospheric composition, but changes in regional land-surface controls, such as the widespread development of thaw lakes, the replacement of tundra by deciduous forest or woodland, and the flooding of the Bering–Chukchi land bridge, were probably also important. We examined the sensitivity of Beringia’s early Holocene climate to these regional-scale controls using a regional climate model (RegCM). Lateral and oceanic boundary conditions were provided by global climate simulations conducted using the GENESIS V2.01 atmospheric general circulation model (AGCM) with a mixed-layer ocean. We carried out two present-day simulations of regional climate – one with modern and one with 11 ka geography – plus

another simulation for 6 ka. In addition, we performed five ~ 11 ka climate simulations, each driven by the same global AGCM boundary conditions: (i) *11 ka Control*, which represents conditions just prior to the major transitions (exposed land bridge, no thaw lakes or wetlands, widespread tundra vegetation), (ii) sea-level rise, which employed present-day continental outlines, (iii) vegetation change, with deciduous needleleaf and deciduous broadleaf boreal vegetation types distributed as suggested by the paleoecological record, (iv) thaw lakes, which used the present-day distribution of lakes and wetlands, and (v) post-11 ka *All*, incorporating all boundary conditions changed in experiments (ii)–(iv). We find that regional-scale controls strongly mediate the climate responses to changes in the large-scale controls, amplifying them in some cases, damping them in others, and, overall, generating considerable spatial heterogeneity in the simulated climate changes. The change from tundra to deciduous woodland produces additional widespread warming in spring and early summer over that induced by the 11 ka insolation regime alone, and lakes and wetlands produce modest and localized cooling in summer and warming in winter. The greatest effect is the flooding of the land bridge and shelves, which produces generally cooler conditions in summer but warmer conditions in winter and is most clearly manifest on the flooded shelves and in eastern Beringia. By 6 ka continued amplification of the seasonal cycle of insolation and loss

of the Laurentide ice sheet produce temperatures similar to or higher than those at 11 ka, plus a longer growing season.

1 Introduction

For the northern high latitudes, climate models simulate significant regional-scale changes that are consistent with presently observed changes in global climate (ACIA, 2004; Serreze et al., 2007) and with projected future global climate changes (e.g., Collins et al., 2013). The distribution and physiological status of vegetation, combined with other features of the terrestrial surface, significantly influence energy, water, and carbon exchange between the land and the atmosphere (e.g., Bonan et al., 1995; Chase et al., 1996; Chapin et al., 2005). Such exchanges produce feedback to local, regional, and global climates, which, in turn, affect plant distribution and physiology (e.g., Thomas and Rowntree, 1992; Foley et al., 1994). Thus, the potential exists for land-cover status to enhance or mitigate climatic change through either positive or negative feedbacks to energy, water, and carbon budgets (Oechel et al., 1993; Lynch et al., 1999; Chapin et al., 2005) and to generate significant feedbacks to the seasonal and annual climatology of much of the Northern Hemisphere.

Large areas of the arctic and subarctic land surface are underlain by continuous or discontinuous permafrost that affects soil and drainage properties. At the landscape scale, land cover is a complex mosaic of tundra (tall shrub, mesic tussock, dry heath, fell-field and barrens, etc.), forest (evergreen conifer, deciduous conifer, and successional hardwoods), wetlands, surface standing water and lakes, and glaciers. Northern ecosystems have received considerable attention in the global budgets of carbon dioxide and methane because soils, peatlands, and lakes are important sources and sinks of these gases and highly sensitive to changes in surface energy exchange (Oechel et al., 1993; Bonan et al., 1995; Zimov et al., 2006; Walter et al., 2006; Walter Anthony et al., 2014). Climatically induced changes in vegetation distribution, especially those involving the replacement of tundra by forest, and changes in soil and permafrost properties will have a dramatic impact on these processes (Smith and Shugart, 1993; Smith et al., 2005). Further, biophysical land–atmosphere coupling via albedo, interactions between vegetation and snow, and modulation of sensible and latent heat fluxes have important climatic implications on seasonal-to-decadal timescales (Harvey, 1988; Thomas and Rowntree, 1992; Bonan et al., 1995; Sturm et al., 2005; Myers-Smith et al., 2011).

Currently observed changes linked to 20th-century warming in the Arctic and subarctic include the expansion of large shrubs in northern Alaskan and Siberian tundra (Sturm et al., 2001, 2005; Forbes et al., 2010), negative trends in evergreen tree growth (Barber et al., 2000; McGuire et al., 2010), and rapidly thawing permafrost (Osterkamp and Romanovsky,

1999; Romanovsky et al., 2010). Vegetation competition–succession model simulations suggest the potential for more extreme shifts from evergreen forest to woody deciduous and/or treeless biomes as a transient response to warming (Chapin and Starfield, 1997). Ultimately these changes and the land–surface interactions inherent in them must be modeled in a realistic way to project future change in the Earth system. One approach for adding to our understanding of the Earth system, and the models used to study it, is to use a set of “natural experiments” based on known past climate changes to evaluate the forcings and feedbacks associated with observed land-cover changes and thus assess climate model sensitivity to such changes. Unglaciated regions of the Arctic warmed early in the Holocene (Kaufman et al., 2004; Miller et al., 2010) and experienced considerable terrestrial change over a few millennia; we use this period to conduct a series of sensitivity experiments with a regional climate model driven by a general circulation model (GCM) simulation for 11 ka.

Beringia (northeastern Siberia, Alaska, and northwestern Canada) is well-suited for such an exercise because a diverse range of paleoenvironmental records is available over the interval from 21 000 yr ago to the present (21 to 0 ka). The early Holocene (ca. 12 to 10 ka) was a time of major climate warming, and paleoenvironmental data document shifts among tundra, woody deciduous and woody evergreen dominance (Edwards et al., 2005). We designed and conducted a series of regional climate model simulations based on observed changes in vegetation, substrate, and sea level in Beringia during the period of major warming centered on the onset of the Holocene (ca. 11 ka). Our primary goal is to assess the sensitivity of the simulated climates to regional land–atmosphere interactions and feedbacks at ca. 11 ka. We also simulated 6 ka conditions, which were climatically more stable but still warmer than present.

1.1 Study area

The regional climate model domain (Fig. 1) is larger than the region typically defined as Beringia (Hopkins, 1982); it encompasses the Indigirka drainage eastward to Chukotka and Kamchatka in the western portion of the study domain and Alaska, a considerable portion of northwest Canada and the adjacent seas in the eastern portion of the study domain. The regional topography is complex, including several mountain ranges, plateaus, low-lying tectonic basins and flat coastal plains. The easternmost parts of the study area lay under the Laurentide ice sheet during the last glaciation; other areas were affected only by local mountain glaciation (Kaufman et al., 2004; Elias and Brigham-Grette, 2007).

The modern climate of the study area has been described by Mock et al. (1998) and Edwards et al. (2001), from which the following description derives. In winter, the climate is influenced by the status of a mid-tropospheric trough–ridge system. An upper-level trough is centered on average to the east of China, and northward of the trough radiational cool-

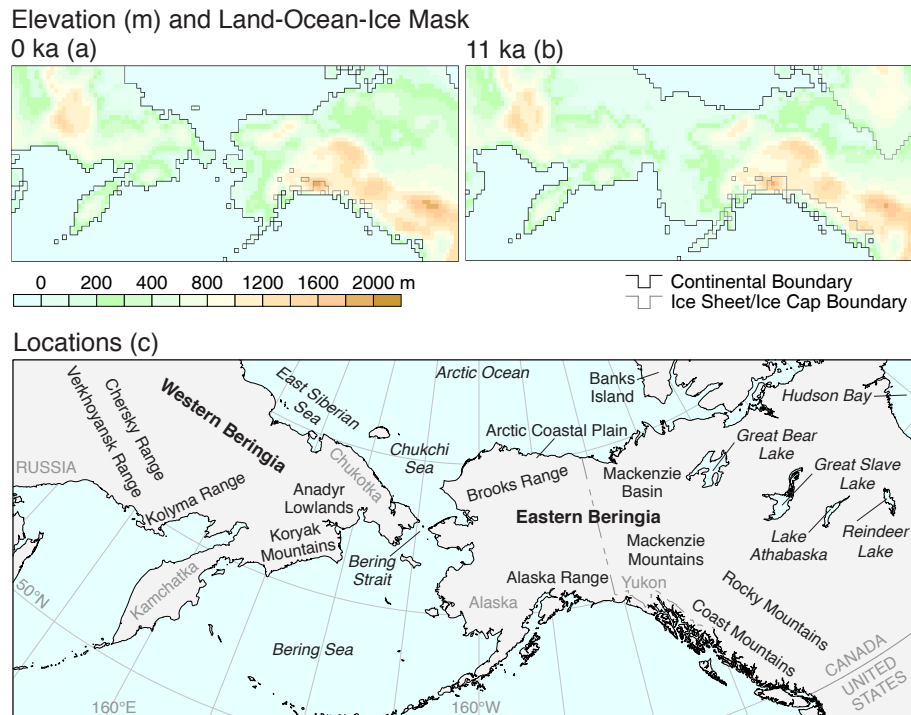


Figure 1. Spatial domain of RegCM for this study showing elevations and coastlines for 0 ka (a) and 11 ka (b). The extent of the Laurentide and Cordilleran ice sheets at 11 ka is indicated by fine grey lines (for ice cover see also Fig. 4). Locations and regions referred to in the text (c).

ing generates a strong surface high over Siberia. Consequent northwesterly winds block the incursion of maritime air into easternmost Asia and are linked to January temperatures as low as -40°C (Mock et al., 1998). High pressure over northwest Canada is associated with cold January temperatures of about -30°C . Conditions are somewhat warmer (-15°C) along the southern coast of Alaska (Mock et al., 1998; Edwards et al., 2001). Summer temperature is driven by high radiation receipts and the advection of warm air into both eastern and western portions of the study area via subtropical high-pressure systems that develop to the south. Summer temperatures range from ~ 5 to 15°C across the study area (Steinhauser, 1979; World Meteorological Organization, 1981). Temperatures generally increase from north to south, except where there is local coastal cooling, and in interior basins of Alaska, which can experience July temperatures of 15°C or higher. In eastern Asia cooler temperatures inland relate to northerly flow due to the position of the East Asian trough over eastern Siberia.

Precipitation is low in winter; inland January total precipitation long-term means may be < 25 mm (Steinhauser, 1979; World Meteorological Organization, 1981), but southern regions of the study area receive abundant orographically enhanced precipitation of 1 m yr^{-1} or more. Typically, there is a late summer precipitation maximum related to midlatitude cyclones that are steered across the region by the East Asian

trough. July precipitation ranges from 50 to 100 mm; in eastern Asia precipitation levels increase southwards, while Alaskan interior basins are generally drier than western or coastal areas.

At a larger scale, the tendency for frequent cyclogenesis over Eurasia, Alaska, and Canada in summer is associated with the development of an Arctic frontal zone. The frequent association of the front with the boreal forest–tundra boundary appears to be related in part to moisture availability and albedo (Pielke and Vidale, 1995; Liess et al., 2012). The front appears most strongly in regions where significant topographic features are contiguous with the ecotone (Lynch et al., 2001). In the absence of large changes in climate, the forest–tundra border may exert a stabilizing effect on regional climate as the relatively high-albedo tundra side of the border will remain cooler than the lower-albedo forest side of the border (Ritchie and Hare, 1971; TEMPO Members, 1996; Lynch et al., 2001). In contrast, when large, externally driven changes in regional climate occur, shifts in the location of the forest–tundra border may locally amplify the climatic change (Foley et al., 1994).

At a regional scale, the distribution of precipitation is strongly influenced by topography, particularly in coastal Alaska and Canada but also in upland regions in the interior (e.g., the Brooks Range), where precipitation is greater than in lowland regions. The same is true in western Beringia,

where precipitation is enhanced in the Chersky, Kolyma, Koryak, and Verkhoyansk mountain ranges and in coastal mountains in the Kamchatka Peninsula.

Land-surface properties also influence local precipitation. For example, the summer precipitation maximum in the Mackenzie Basin is associated with a minimum in large-scale vapor-flux convergence (Walsh et al., 1994), suggesting that substantial summer precipitation is derived from within-basin recycling of water vapor via evapotranspiration from the tundra and boreal forest. The numerous Alaskan lakes have a strong effect on surface fluxes and heat storage (Oncley et al., 1997; Rivers and Lynch, 2004), and it is possible that widespread fields of lakes that characterize some parts of the region may be an important source of feedback at the regional level (Subin et al., 2012).

Modern vegetation is a mosaic of forest and tundra communities. The northern Siberian coastlands, western and northern Alaska, Banks Island and the Canadian Beaufort Sea coastlands are characterized by tundra. Shrubs of varying stature dominate in many areas, but grasses and sedges characterize wet coastal zones. Alpine tundra occurs above boreal forest tree line at altitudes over 500–800 m. Forests in the Asian portion of the study region are dominated by the deciduous conifer *Larix cajanderi* (Dahurian larch; synonyms *L. gmelinii* and *L. dahurica*). River valleys also support gallery forests of *Populus suaveolens* (Mongolian poplar) and *Chosenia arbutifolia* (Korean willow). *Populus tremula* (quaking aspen) and various species of tree *Betula* can occur as pure stands on slopes or mixed within conifer communities. The shrubby stone pine, *Pinus pumila*, forms areas of shrub tundra in northeastern Siberia and is a common understory component of larch forests.

The evergreen conifers, *Picea glauca* and *P. mariana* (white and black spruce), dominate forests in Alaska and northern Canada; here, hardwoods such as *Populus tremuloides* and *P. balsamifera* (aspen, balsam poplar) and *Betula neoalaskana* and *B. papyrifera* (paper birch) form seral stands after disturbances such as fire. Permafrost is continuous in the north and discontinuous to the south of the region (Rekacewicz, 1998). Extensive wetlands occur across the region related to topography and permafrost-impaired drainage. The southeastern part of the study area includes grassland and shrubland of the Columbia Plateau and interior Canada.

1.2 Key changes in land-cover features during deglacial warming

At the last glacial maximum (LGM: 25–18 ka) global sea level was lowered by ~120–135 m (Fairbanks, 1989; Yokoyama et al., 2000). The shelves of the Bering and Chukchi Seas and Arctic Ocean were exposed, and Alaska and Siberia formed a continuous land mass. The Laurentide and Cordilleran ice sheets (LIS, CIS) lay to the east and southeast of Beringia, and mountain glaciations occurred

in the Brooks, Chersky, Kolyma, Koryak, and Verkhoyansk mountain ranges and other upland regions. Considerable eolian deposition occurred in lowland areas, particularly in the northern coastal plain of Siberia, the Anadyr lowlands, and interior basins and the northern coastal plains of Alaska and Canada (Hopkins, 1982).

By 11 ka, rapidly melting continental ice sheets (and the large-scale atmospheric circulation changes associated with them), rising sea level, and increasing summer insolation generated a series of terrestrial changes in Beringia (Kaufman et al., 2004). Sea level rose rapidly during deglaciation (Fairbanks, 1989); estimates suggest that the Bering Strait formed about 11 ka, but several millennia passed before the remaining expanses of exposed continental shelf were completely inundated (Manley, 2002; Keigwin et al., 2006). Beginning 15–14 ka, rates of thermokarst erosion increased, creating thaw lakes in low-lying regions underlain by frozen, unconsolidated substrates, such as exposed shelves, large floodplains, and loess-blanketed regions (Hopkins, 1949; Williams and Yeend, 1979; Burn, 1997; Romanovskii et al., 2000; Walter et al., 2007). This period also marked the inception of wetlands and peat growth, which developed further in subsequent millennia (Jones and Yu, 2010). Thaw-lake formation accelerated in the early Holocene after 11 ka but decreased subsequently (Walter et al., 2007; Walter Anthony et al., 2014). It is likely that the current proportion of land occupied by lakes (for example 5–40 % on the Arctic coastal plain) was attained during the early Holocene (Walter et al., 2007).

Over the period from ca. 15 to 8 ka, a sequence of changes in zonal vegetation occurred in Beringia. Across the region, graminoid-forb tundra that typified the LGM was replaced, around 15–14 ka, by *Salix*- and *Betula*-dominated shrub tundra, generally interpreted to be initially of low stature (Anderson et al., 2004; Edwards et al., 2005). Over the next few millennia much of the region became dominated by woody taxa, although the species composition differed between the Asian and North American sectors. Between ca. 13 and 10 ka, lower-elevation regions of unglaciated Alaska and Canada saw the expansion of deciduous tall-shrub and woodland vegetation; in Asia at this time vegetation cover at lower elevations included deciduous shrubs and hardwood trees such as *Betula platyphylla* (Asian birch), with *Larix* in the western portion of the region (Edwards et al., 2005). Between ca. 11 and 10 ka evergreen conifer forest developed in the eastern sector. The evergreen *Pinus pumila* spread across the western sector, within and beyond the *Larix* forest limits. Shrub tundra remained dominant north of the tree line across the whole region, except in the far north, where dwarf shrub or herb-dominated tundra occurred. These general vegetation features persist to the present day, although there have been subtle changes in tree limits and forest composition (Anderson et al., 2004).

We focused on three features of 11 ka land-cover change for our model experiments: (i) the change in paleogeography

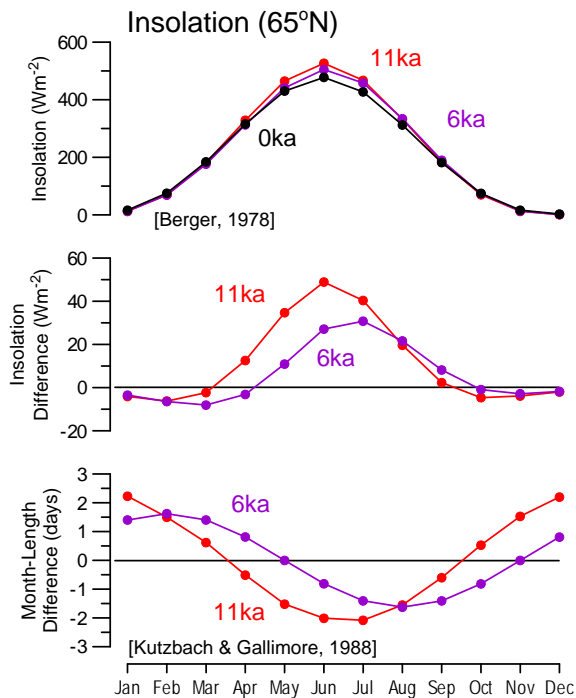


Figure 2. Monthly insolation at present (0 ka), 6 and 11 ka after Berger (1978; upper); insolation differences between present and 6 and 11 ka (middle); month-length differences between present and 6 and 11 ka (lower). The shorter summers and longer winters at 6 and 11 ka (relative to present) arise from the elliptical orbit of the Earth and the precession of the equinoxes (see Kutzbach and Gallimore, 1988).

caused by the flooding of the Bering land bridge and continental shelves, (ii) the change in vegetation represented by a shift from low-stature shrub tundra typical of early deglaciation to deciduous tall-shrub and woodland vegetation, and (iii) the development of wetlands and fields of thaw lakes across low-lying terrain. We additionally examined the output from a simulation for 6 ka, a time when insolation patterns were still markedly different from present (Fig. 2) but land cover and continental outlines were similar to present.

2 Methods

2.1 Climate models

We used a hierarchical modeling procedure that involves running an atmospheric general circulation model (AGCM) to simulate global climate and provide time series of sea-surface temperature (SST), sea ice, and lateral boundary conditions (vertical profiles of temperature, wind, humidity) for the regional climate model (RCM) simulations. In previous studies, this hierarchy of models has been demonstrated to reproduce present-day climate and simulate regional-scale responses to changes in the large-scale controls that compare favorably with reconstructions of those responses from paleo-

oenvironmental data (Hostetler and Bartlein, 1999; Hostetler et al., 1994, 2000). This method of coupling GCMs with RCMs to downscale climate is now widely used in climate assessments (e.g., Mearns et al., 2012).

The AGCM is version 2.01 of the GENESIS climate model (Thompson and Pollard, 1995). Version 2.01 and later versions of GENESIS have been used extensively for paleoclimate simulations (Pollard and Thompson, 1997; Joussaume et al., 1999; Pinot et al., 1999; Ruddiman et al., 2005; Tabor et al., 2014; Alder and Hostetler, 2015). The atmospheric component of GENESIS is coupled with the Land Surface eXchange model (LSX; Thompson and Pollard, 1995), to simulate surface processes and to account for the exchange of energy, mass and momentum between the land surface and the atmospheric boundary layer. We used model resolutions of T31 ($\sim 3.7^\circ$ in latitude and longitude) and $2^\circ \times 2^\circ$ in latitude and longitude for the atmosphere and surface, respectively. The model was run using a coupled mixed-layer ocean (50 m in depth), which produces SSTs in radiative balance with global boundary conditions. We ran a number of sensitivity experiments in which we varied sea-ice parameters to optimize the simulation of present-day sea ice. The boundary conditions for the RegCM simulations span the last 10 yr of 65 yr long GENESIS simulations.

The RCM is version two of the RegCM regional climate model (RegCM2; Giorgi et al., 1993a, b). Newer versions of RegCM now exist that offer more options and improved computational performance (Pal et al., 2007), but the atmospheric core of the model has remained essentially the same as in RegCM2. Our version of RegCM2 is coupled with the LSX surface-physics package used in GENESIS. We employed a model grid resolution of 60 km (roughly 0.5°) for the simulations (Fig. 1a and b). To optimize our sensitivity tests we modified RegCM2 to include orbitally determined insolation and a lake model (Hostetler and Bartlein, 1990) to simulate lake temperature and ice and their feedbacks with the boundary layer. We also modified aerodynamic (e.g., roughness height) and biophysical (e.g., leaf area index) vegetation parameters in LSX to be consistent with the properties of the reconstructed Beringia vegetation. For the lake sensitivity tests, we represented the spatial distribution of shallow thaw lakes by specifying time-appropriate (i.e., 0, 6 and 11 ka) model grid points as water. For all lakes, we specified a depth of 4 m and moderately high turbidity, which is sufficient to realistically capture the seasonal cycle of lake–atmosphere feedbacks in our experiments. The vegetation and lake implementations are discussed in more detail below. Each RegCM2 simulation was run for 10 yr and the first 2 yr are excluded from our analysis to allow soil-moisture fields to equilibrate. Ten-year simulations with 8 yr averages are sufficient to allow for model spin-up and to isolate mean climate responses associated with our array of prescribed changes in paleogeography, which, in most cases, represent substantial perturbations between and among experiments. In contrast to GCMs, where time-slice simulations may take tens to hun-

dreds of years to reach equilibrium, RCM simulations reach equilibrium rapidly under the strong external forcing of the GCM.

Large-scale, lateral boundary conditions (temperature, humidity, wind, surface pressure and SSTs) from the GCM are provided to the RCM every 6 h, and do not vary within the interval. There is a 12-grid-point “sponge” region on all sides of the RCM domain where the GCM boundary conditions are exponentially relaxed as they are introduced. The RCM simulates the full dynamics of weather and climate in the interior of the domain. To the extent possible, the characteristics of the exit flow (here generally out of the eastern boundary) are matched to the GCM. Some RCMs use a spectral nudging technique within the RCM domain to constrain tropospheric flow within the entire domain to match the GCM flow closely; nudging is not implemented in RegCM2. Moisture is conserved within the domain of the RCM. RegCM2 includes the Biosphere Atmosphere Transfer Scheme (BATS) surface physics package. Land use and vegetation types determine the specified values of a number of biophysical and physical parameters in BATS such as albedo, roughness length, stomatal resistance, and rooting depth. Changing land use types thus changes the associated parameters which in turn alters feedbacks in the boundary layer and leads to climate responses that will become evident in the simulations.

It is our experience that if the RCM domain is correctly placed so as to capture the important circulation characteristics of the region of interest that the simulated climates of the GCM and RCM are similar over the RCM domain; however, the higher resolution of features such as mountain ranges in the RCM can result in differences and improvements in the location and amplitude of related climate fields such as air temperature and precipitation. It is also the case that the RCM has limited ability to correct for deficiencies in the GCM forcing fields. For example, if the 500 hPa flow along the domain border is misplaced in the GCM, that displacement will propagate to the RCM.

2.2 Experimental design

We designed our experiments to isolate and quantify the potential controls of the early Holocene climate of Beringia. Our experiments thus include a set of varied atmospheric boundary conditions and surface changes that we describe and summarize below.

2.2.1 Present-day, 6 and 11 ka boundary conditions

The AGCM and RCM each require the specification of insolation, surface boundary conditions (including 11 ka continental outlines and land-surface and ice-sheet topography), atmospheric greenhouse gas composition, land-cover (vegetation and soils), and lake and wetland distribution (Table 1). Insolation for present, 6 and 11 ka was specified following Berger (1978; Fig. 2). Atmospheric composition (e.g., CO₂)

was set to preindustrial values (i.e., 280 ppm) for the *Present Day* and *6 ka* simulations, and to 265 ppm (Monnin et al., 2001) for the 11 ka simulations.

The impact of the variations in the obliquity (tilt) and climatic-precession (time of year of perihelion) elements of the Earth’s orbit can be seen in the anomalies of insolation and the lengths of the different months and seasons (Berger, 1978; Kutzbach and Gallimore, 1988; Fig. 2). At 11 ka, perihelion was in late June, the tilt of the Earth’s axis was 24.2°, and the eccentricity was about 0.019 (as compared to the present values of early January, 23.4°, and 0.017). Consequently, June insolation was about 50 W m⁻² greater than present at 65° N. However, owing to its elliptical orbit, the Earth moves faster near the time of perihelion (Kepler’s law of equal areas), and at 11 ka June and July were about 2.0 days shorter than present (assuming a 360-day year and 30-day months; Kutzbach and Gallimore, 1988). At 6 ka, perihelion was in September, the tilt was 24.1°, and eccentricity was about the same as at 11 ka. The maximum insolation anomaly consequently occurred later, in July, and was about 30 W m⁻² greater than present at 65° N. Owing to the later time-of-year of perihelion at 6 ka than at 11 ka, August was the shortest month (1.65 days shorter than present). From Fig. 2 it can be seen that in February and August, both insolation and month-length anomalies for 11 and 6 ka were similar. Overall, the early-Holocene boreal summer and the mid-Holocene late summer could be described as shorter and “hotter” than at present.

Figure 1 shows the 0 ka (present) and 11 ka topography, ice and continental outlines. Ice-sheet elevations for the 11 ka AGCM simulation were derived from Peltier (1994) and from Hostetler et al. (2000) for the 11 ka RCM simulations. Land-surface elevations (and hence the continental outlines) were specified for each model at 11 ka by interpolating Peltier (1994) ICE-4G topographic anomalies (i.e., 11 ka minus 0 ka differences) and applying these to the present-day grid point elevation in the model. In the RCM at 11 ka, this procedure yields a land mask with an extensive land bridge between North America and Asia (Fig. 1b). We constructed a second set of land elevations to depict the flooded land bridge by superimposing the present-day land mask over the 11 ka elevations and setting all values outside of the present-day shoreline mask to sea level (0.0 m; Fig. 1a). Because the topography in the region consists of either broad coastal plains with low slopes or rather steep terrain in coastal mountain regions, we did not need to “taper” the coastal elevations when creating this elevation data set.

Land-cover characteristics were expressed in both models as Dorman–Sellers “biome” types (Dorman and Sellers, 1989), which implicitly include the specification of soil characteristics associated with the vegetation. For the AGCM simulation these biomes closely followed Lynch et al. (2003). For the RCM simulations, present-day land-cover characteristics (including wetlands) were derived from the Global Land Cover Characteristics database

Table 1. Simulation boundary conditions and land cover.

Simulation name	Insolation	CO ₂ (ppm)	Vegetation	Lakes	Continental outlines	Topography and ice	Supplement figure
<i>Present Day</i> ¹	Modern	280	Modern	Modern	Modern	Modern	1
<i>Present Day with 11 ka Continental Outlines</i> ²	Modern	280	Modern	Modern	11 ka	11 ka topography only	2
<i>11 ka Control</i> ³	11 ka	265	Shrub tundra (~ 13 ka)	No lakes	11 ka	11 ka	4
<i>11 ka Sea Level</i> ^{4,5}	11 ka	265	Shrub tundra (~ 13 ka)	No lakes	Modern	11 ka modified	7
<i>11 ka Vegetation</i> ⁶	11 ka	265	Deciduous shrub or woodland (11 ka)	No lakes	11 ka	11 ka	9
<i>11 ka Lakes</i>	11 ka	265	Shrub tundra (~ 13 ka)	Modern	11 ka	11 ka	11
<i>11 ka All</i> ^{6,7}	11 ka	265	Deciduous shrub or woodland (11 ka)	Modern	Modern	11 ka modified	13
<i>6 ka</i>	6 ka	280	Modern	Modern	Modern	Modern	16

¹ Vegetation is slightly simplified from the GLCC BATS values. ² Continental outlines and topography were adopted from the *11 ka Control* simulation, along with land cover from the *Present Day* simulation. ³ The 11 ka “point of departure” for 11 ka vegetation, lakes, and shelf-flooding experiments. Shrub tundra represents vegetation prior to 11 ka (~ 13 ka). ⁴ Vegetation is from the *11 ka Control* simulation. Modern continental outlines. ⁵ The 11 ka modified topography is 11 ka topography (modern topography + Peltier anomalies), with grid points that would be ocean at the present day set equal to 0 m. ⁶ Vegetation includes large areas of deciduous tall shrub and woodland. ⁷ Effect of all three changes (in vegetation, lake distribution and sea level) from just before 11 ka (shrub tundra, no lakes, exposed shelf) to just after (deciduous shrub and/or woodland, lakes, flooded shelf).

(http://edc2.usgs.gov/glcc/globdoc2_0.php). The spatial pattern of the land-cover types was simplified to create general patterns at the same spatial resolution of information available from paleorecords for describing the 11 ka land-cover type patterns, including wetlands (Figs. 3 and 4). We further specified the distribution of shallow thaw lakes, and, to represent the short-stature deciduous tall-shrub and/or woodland vegetation in the early Holocene (“deciduous broadleaf woodland”; Fig. 3), we defined an additional land-cover type for which we specified appropriate vegetation-type parameter values in LSX (e.g., leaf-area index, canopy structure and height).

2.2.2 Present-day, 6 and 11 ka surface characteristics

Surface characteristics describing land cover, sea level and the distribution of lakes and wetlands were defined for the present-day, 6 and 11 ka RCM simulations. For the 11 ka RCM simulations, we used five separate sets of surface characteristics (land mask, topography, and land-cover type) that are described in detail below. The first set represents conditions prior to 11 ka, and represents the “point of departure” for the 11 ka experiments (and hence is referred to here as the *11 ka Control*). A second set represents conditions after the 11 ka changes (referred to here as *11 ka All*). Three other sets were defined to examine the individual effects of land-bridge flooding (*11 ka Sea Level*), vegetation change from tundra to deciduous tall shrub and/or woodland (*11 ka Vegetation*), and thaw-lake and/or wetland development (*11 ka Lakes*; Fig. 4b–f; Table 1). In each case, paleoenvironmental data indicate that full development of the sea level, vegetation, and thaw-lake and/or wetland changes took centuries to millennia, the marine transgression being the most long-

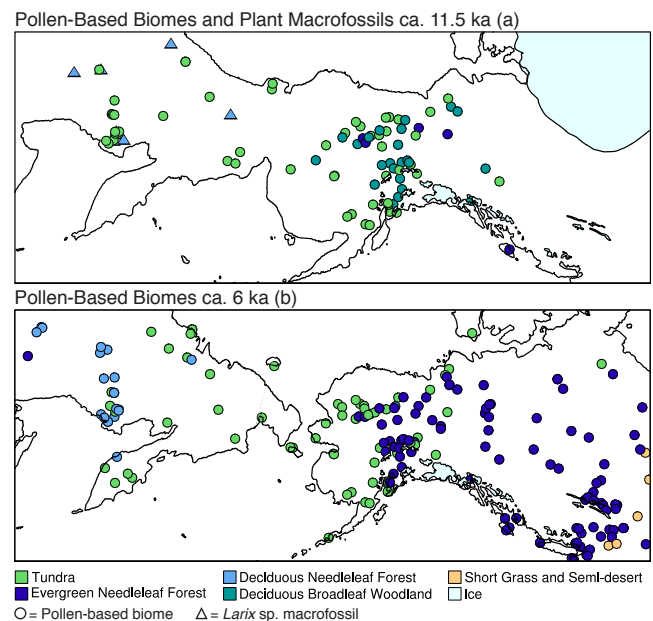


Figure 3. Pollen-based biomes for ca. 11.5 ka (a; this study) and ca. 6 ka (b; from Prentice et al., 2000; Bigelow et al., 2003). The 11.5 ka pollen patterns indicate deciduous broadleaf woodland in Alaska and Canada (a), but in Siberia this biome is identified from macrofossils only (not shown; see Sect. 2.2.8). At 6 ka deciduous needleleaf forest in Siberia is identified from widespread *Larix* pollen. The main difference between 6 ka and modern is the truncated distribution of evergreen needleleaf forest in western Alaska at 6 ka. Biome identities and colors map onto the RegCM land-cover PFTs (plant functional types) in Fig. 4. Ice from Dyke et al. (2003) and coastline inferred from Peltier (1994) topographic anomalies.

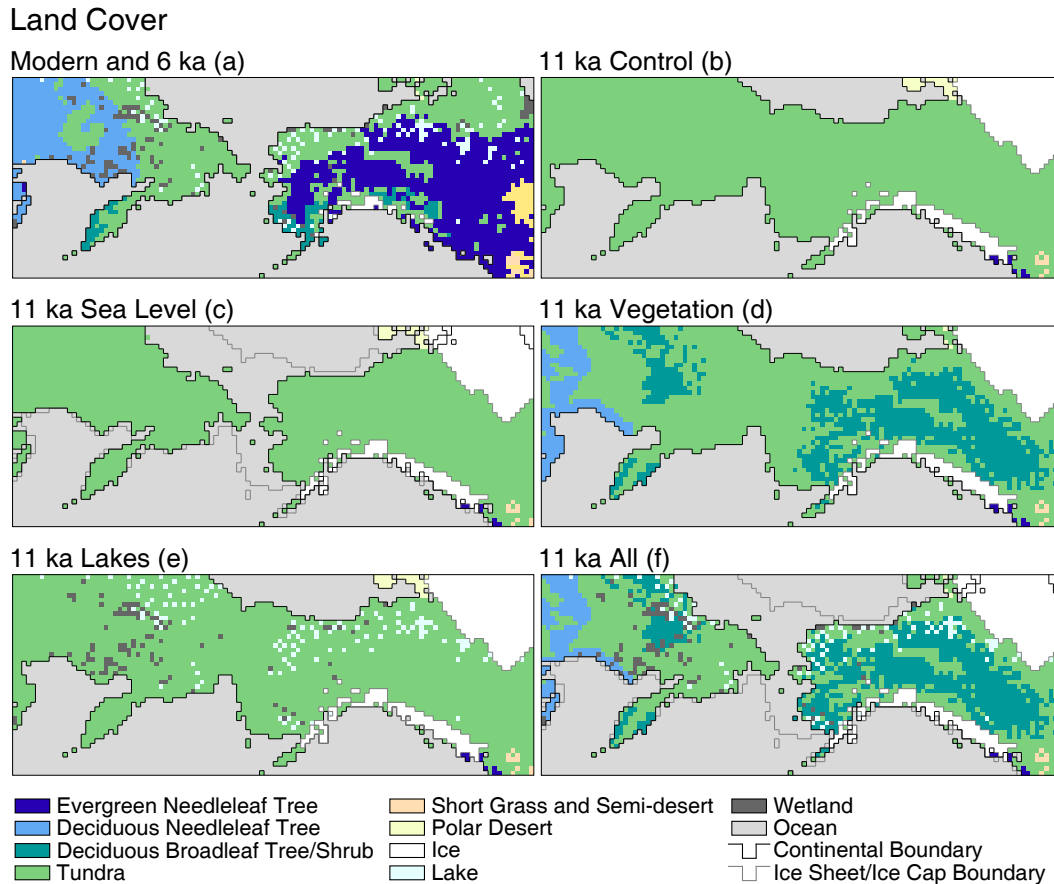


Figure 4. Land cover for RegCM climate simulations. Modern conditions are also used for the 6 ka simulation; there are minor differences in forest cover between modern conditions and 6 ka (see Fig. 3). The vegetation cover in each simulation is represented by the set of RegCM plant functional types (PFTs); the PFT Deciduous Broadleaf Tree/Shrub was created to represent the characteristics of short-statured deciduous woodland and tall-shrub communities. Land cover for 11 ka All (f) combines all three experimental land-cover changes. Each land-cover map is linked to a RegCM simulation; an additional simulation was made using modern land cover with 11 ka continental outlines (not shown).

lived. However, as our study features an equilibrium sensitivity experiment, we created just two steady states of 11 ka land cover, representing conditions close to the onset of changes (11 ka Control) and conditions when all the changes were fully expressed (11 ka All). We also defined two sets of surface characteristics for the present day, in order to separate the effects of land-bridge flooding from the other boundary-condition changes.

2.2.3 Present Day simulation

The *Present Day* (0 ka) simulation land cover included modern vegetation (Fig. 4a) defined as a mosaic of tundra and needleleaf forest (as described in Sect. 1.1), with short-grass and semi-desert vegetation in the extreme southeast of the study area. The modern distribution of lakes and wetlands was used, as were modern topography and continental outlines, which created a land mask with the modern Bering Strait between Asia and North America.

2.2.4 Present-day simulation with an 11 ka land mask

We defined a second set of present-day boundary conditions by combining the modern land-cover data with an 11 ka land mask including elevation data. This set of boundary conditions is used to separate the simple effects of the land-bridge flooding from the combined effects of all of the other “paleo” boundary conditions.

2.2.5 6 ka simulation

We also used modern land cover (Fig. 4a) for the 6 ka simulation. Lakes and wetlands were well established at 6 ka (Walter et al., 2007; Jones and Yu, 2010). Pollen-based biomes for 6 ka defined by the BIOME 6000 project (Prentice et al., 2000; Edwards et al., 2000a; Bigelow et al., 2003) were used as a guide to vegetation cover. In Siberia, the modern land cover (Fig. 4a) closely approximates the 6 ka biome distribution (Fig. 3b), while in eastern Beringia the western ever-

green needleleaf forest limit is displaced eastwards. Almost all post-glacial sea-level rise had occurred by 6 ka (Manley, 2002) and the continental outlines are only slightly different from modern outlines (as shown in Fig. 3b); we considered the vegetation and coastline differences not significant enough to require a separate 6 ka land cover mask.

2.2.6 11 ka Control simulation

The late-glacial development of Beringian vegetation proceeded over several millennia from herbaceous vegetation through low shrubs to tall shrubs and deciduous woodland (see Sect. 1.2). We use the low-shrub tundra to represent the vegetation for the 11 ka Control simulation; its surface properties differ little from the preceding herbaceous tundra vegetation (not modeled here). We also included the 11 ka LIS, CIS, and mountain glaciers and ice caps but not lakes and wetlands (Fig. 4b). Topography was defined using Peltier (1994) 11 ka geography and by adding the paleotopographic anomalies to the present-day elevations. The resultant RCM land mask features a lower sea level, with the Bering land bridge in place between Asia and North America (see Sect. 2.2.1), and 11 ka land and ice topography.

2.2.7 Sea-Level simulation

The 11 ka Sea Level simulation was identical to the 11 ka Control simulation, but with topography defined using Peltier (1994) 11 ka geography and modern sea level (Fig. 4b and c; see Sect. 2.2.1). This combination created an RCM land mask with 11 ka topography but a flooded land bridge (i.e., the modern Bering Strait) between Asia and North America.

2.2.8 Vegetation simulation

The 11 ka Vegetation simulation was identical to the 11 ka Control simulation with the exception of vegetation (Fig. 4d). To describe the changed vegetation for this simulation we used an approach involving several steps: the “biomization” of pollen data (Prentice and Webb, 1998; Bigelow et al., 2003), evidence from plant macrofossils (Edwards et al., 2005; Binney et al., 2009) and expert knowledge. The latter was needed because the biomized pollen maps and macrofossil records (Fig. 3) indicate broad trends in vegetation cover but hold too few data points to allow for quantitative spatial interpolation. We used records from the PARCS (Paleoenvironmental Arctic Sciences) database (<http://www.ncdc.noaa.gov/paleo/parcs/index.html>) falling nearest to 11.5 ka in age to guide the placement of deciduous broadleaf woodland for the 11 ka Vegetation simulation. This time slice gave the strongest signal of deciduous woodland in eastern Beringia, defining the deciduous broadleaf woodland biome at about half the sites across the region. Deciduous needleleaf (*Larix*) forest is not identified in far northeast

Siberia at 11 ka by biomized pollen maps, likely due to low *Larix* pollen counts in the data; not even enhancing *Larix* by a factor of 15 (see Bigelow et al., 2003) identifies deciduous needleleaf forest at this time. However, the macrofossil record indicates the presence of deciduous broadleaf trees in east and west Beringia and of *Larix* in Siberia (Edwards et al., 2005; Binney et al., 2009; Fig. 3). Based on these data, in east Beringia we specified 11 ka vegetation as a mosaic of low-stature shrub tundra and deciduous tall shrub and/or woodland, with the latter occupying lower elevations. In west Beringia we specified 11 ka vegetation as a mosaic of low-stature shrub tundra and mixed deciduous woodland, also determined by elevation. We designated the exposed shelf and land bridge as low-stature shrub tundra, as in the 11 ka Control simulation, as little is known about past vegetation of the submerged land areas at ca. 11 ka; pollen and macrofossil data from terrestrial and submarine sediment cores taken from the Bering Sea suggest shrub tundra (e.g., Elias et al., 1997; Ager and Phillips, 2008; Lozhkin et al., 2011).

2.2.9 Lakes simulation

The 11 ka Lakes simulation was identical to the 11 ka Control simulation with the exception of lake and wetland cover. For the 11 ka Control simulation, no lakes or wetlands were present on the RCM land cover grid. For the 11 ka Lakes simulation, lakes and wetlands were represented by their modern distributions, placing lakes in regions where thaw lakes dominate the modern landscape (Fig. 4e). Lake and wetland distributions are derived from the Global Land Cover Characteristics database described above. Thaw lakes probably extended onto Arctic Ocean shelves (Hill and Solomon, 1999; Romanovskii et al., 2000) that are now inundated, and they probably also formed on the land bridge, but, as there is no information on their areal extent, we omitted lakes from these areas. The estimated average percent cover of lakes in modern lake-dominated landscapes from topographic maps and air photos is 5–40%. In the experiment we used 40% in order to provide the maximum possibility for a response in the simulation. Although thaw lakes are typically <1.0 to a few kilometers in diameter, the structure of the RCM necessitated that lakes were assigned as whole grid cells according to the same proportions.

2.3 Summary

Our strategy was to examine a set of RCM simulations for 11 ka (Table 1) that together illustrate the impact of changes in vegetation, flooding of the land bridge, and development of thaw lakes and wetlands. We compared these 11 ka simulations with the 11 ka Control simulation and with simulations of the present day and 6 ka, to generate a set of experiments (Table 2).

The simulations (described above; Table 1) can be summarized as follows:

1. *Present Day* – a simulation of the present day (0 ka) with realistic land cover (including vegetation, shorelines, and thaw-lake distribution). This is the control simulation used to compare changes between 11 ka and present (Fig. 4a).
2. *Present Day with 11 ka Continental Outlines* – a simulation which used present climatology, vegetation and lakes/wetlands but the 11 ka continental outlines (i.e., Fig. 4a but with continental outlines as in Fig. 4b). This simulation is used to partition the effect of changed sea level from that of other key drivers, such as insolation.
3. *11 ka Control* – a simulation of conditions that prevailed prior to the changes in vegetation, sea level, and thaw-lake distributions that are the focus of the study. This simulation functions as the control simulation against which the effects of these land-cover changes at 11 ka are assessed (Fig. 4b).
- 4.–6. Three simulations – *11 ka Sea Level*, *11 ka Vegetation*, and *11 ka Lakes* – which address each land-cover change in isolation (Fig. 4c–e).
7. *11 ka All* – a simulation with all three land-cover changes (i.e., sea level, vegetation, lakes) included (Fig. 4f) to illustrate the combined effects of these controls.
8. *6 ka* – a simulation using 6 ka boundary conditions and modern land cover (Fig. 4a) to explore a climate with modern boundary conditions, except for an amplified annual cycle of insolation.

The experiments (Table 2) were as follows:

1. *Present Day* minus *Present Day with 11 ka Continental Outlines*, which assesses the effect of the Bering Strait and modern coastline on modern climatology.
2. *11 ka Control* minus *Present Day*, which describes the full change in conditions from 11 ka (before land-cover transformation) to modern conditions (including the imposition of the Bering Strait).
3. *11 ka Control* minus *Present Day with 11 ka Continental Outlines*, which reveals the effect of insolation on the 11 ka climatology, as the large impact of sea-level change in the fully modern (*Present Day*) simulation is removed by using the 11 ka continental outlines.
- 4.–7. Three experiments to examine the one-at-a-time changes in sea level, vegetation, and thaw lakes and one experiment to examine the effect of all three of the above changes. The control in each case is *11 ka Control*.

8. *11 ka All* minus *Present Day*, which describes the full change in conditions from 11 ka (after land-cover transformation and including the imposition of the Bering Strait) to modern conditions.
9. *6 ka* minus *Present Day*, which examines the impact of mid-Holocene insolation anomalies.
10. *6 ka* minus *11 ka All*, which examines the climate change between 11 and 6 ka.

An experimental design that focuses on higher-order interactions among the controls would be theoretically possible but would require many more simulations. We elected to keep the experimental design relatively simple.

3 Results

We present the modeling results in a series of figures that typically take the form of mapped monthly averages. Monthly averages are based on a 365-day year relative to the modern calendar (the effects of the “calendar bias” (Sect. 2.2.1) are of continental and hemispheric scales and would not dominate the regional patterns of interest here; Timm et al., 2008). In some cases the complete annual cycle is shown, in others summer and winter months (e.g., January and July) that highlight the more interesting patterns that emerge from the simulations. Maps representing the results of specific simulations show 8 yr climatologies; those showing the results of experiments display differences between experimental and control simulation long-term means (i.e., anomalies). Maps of all monthly values of key variables are available in the supporting online information (see Supplement).

Overall, the RCM simulations are in good agreement with the (global) GCM simulations for the region (not shown), a natural consequence of the way in which the lateral boundary conditions are supplied to the regional model. The general changes in climate between 11 or 6 ka and present are driven by large- or global-scale changes in such controls as insolation, atmospheric composition, changes in continental outlines (as influenced by changing sea level), and changes in the area and height of the ice sheets; these are controls that influence the response of the GCM and RCM in similar ways. Likewise, SSTs strongly influence regional climates, and in our simulations, these values are identical in the GCM and RCM.

3.1 Effect of the land-bridge flooding alone

The effect of the land-bridge flooding alone (i.e., with no other differences in boundary conditions between 11 ka and present) is assessed by the experiment that replaces the modern land mask and elevation with one appropriate for 11 ka. For reference, Fig. 5a shows the simulated modern monthly average air temperature for the study area. Figure 5b shows

Table 2. Experiments.

Experiment	Control	Description	Supplement figure
<i>Present Day</i>	<i>Present Day with 11 ka Continental Outlines</i>	Impact of 11 ka land bridge and continental outlines at present	3
<i>11 ka Control</i>	<i>Present Day</i>	Impact of (pre-) 11 ka continental outlines, vegetation, lakes and wetlands and 11 ka ice, topography, insolation, and CO ₂ (relative to present)	5
<i>11 ka Control</i>	<i>Present Day with 11 ka Continental Outlines</i>	Impact as above except for continental outlines	6
<i>11 ka Sea Level</i>	<i>11 ka Control</i>	Impact of land-bridge flooding at 11 ka	8
<i>11 ka Vegetation</i>	<i>11 ka Control</i>	Impact of change from shrub tundra to deciduous woodland at 11 ka	10
<i>11 ka Lakes</i>	<i>11 ka Control</i>	Impact of thaw-lake development at 11 ka	12
<i>11 ka All</i>	<i>11 ka Control</i>	Impact of sea level, vegetation and lake changes at 11 ka	14
<i>11 ka All</i>	<i>Present Day</i>	Impact of 11 ka continental outlines (flooded land bridge), vegetation, lakes and wetlands, ice, topography, insolation, and CO ₂ (relative to present)	15
<i>6 ka</i>	<i>Present Day</i>	Impact of 6 ka insolation (relative to present)	17
<i>6 ka</i>	<i>11 ka All</i>	Impact of changing insolation and CO ₂ between 11 ka and 6 ka	18

the impact on modern climate of “restoring” the 11 ka continental outlines (and topography). The anomalies shown are the long-term mean differences of the *Present Day* simulation (Fig. S1 in the Supplement) minus the *Present Day with 11 ka Continental Outlines* simulation (Fig. S2). The anomalies show the impact that flooding of the land bridge (and related topographical changes, such as the collapse of the ice sheet) would have on the modern climate if those paleogeographic changes occurred today (Fig. S3).

The prominent effect of shelf flooding is a reduction in the seasonality of 2 m air temperatures as a result of replacing land with ocean. Warm-season (May to October) temperature anomalies are strongly negative, particularly in those regions that are ocean with sea ice in the *Present Day* simulation but which are land in the *Present Day with 11 ka Continental Outlines* simulation (Fig. 5b). In the cool season (November through April) the temperature anomalies are strongly positive in the regions that are oceans in the *Present Day* simulation but land in the *Present Day with 11 ka Continental Outlines* simulation. (The impact of the decrease in elevation of the region that was ice-covered at 11 ka is visible as a small area of positive summer temperature anomalies in the northeastern corner of the model domain.)

The genesis of these temperature anomalies lies in changes in the surface energy balance related to large differences in the heat capacity and albedo of land and water in the two present-day simulations (Fig. S3b). Net shortwave radiation anomalies are highly negative from May through August in the regions that change from land to ocean. This pattern shows the response to the large increase in albedo as dark

land surfaces are replaced by ocean and permanent or seasonal sea ice. Positive net shortwave radiation anomalies occur over the region associated with the 11 ka ice sheet where elevation decreases. While present-day land cover is used in both simulations, the higher elevations in the *Present Day with 11 ka Continental Outlines* simulation result in a persistent snowpack in the northeastern part of the study area. Consequently, simulated net shortwave radiation is lower than present (thereby producing the positive anomalies). Net shortwave anomalies in the cool season (November through March) are close to 0, consistent with the low shortwave radiation inputs at that time of year.

Net longwave radiation anomalies in the warm season are positive where 2 m air temperatures are negative (Fig. S3b), indicating a smaller upward component of longwave radiation. From November to March, net longwave anomalies are strongly negative where 2 m air temperature anomalies are positive, indicating a greater upward component of longwave radiation. Net radiation anomalies follow those of net longwave radiation in the cool season and form a mosaic of anomalies of different sign at other times during the year.

Among the non-radiative components, the anomalies of heat flux into or out of the substrate (i.e., into or out of storage) are most strongly expressed in the region where ocean replaces land. Strong positive anomalies prevail from June through August (Fig. S3b), as energy is stored in the soil during the warm season. Anomalies are strongly negative in the cool season (i.e., greater flow from the substrate to the surface). In the winter the formation of sea ice does not appreciably diminish the flow of energy out of storage. The anoma-

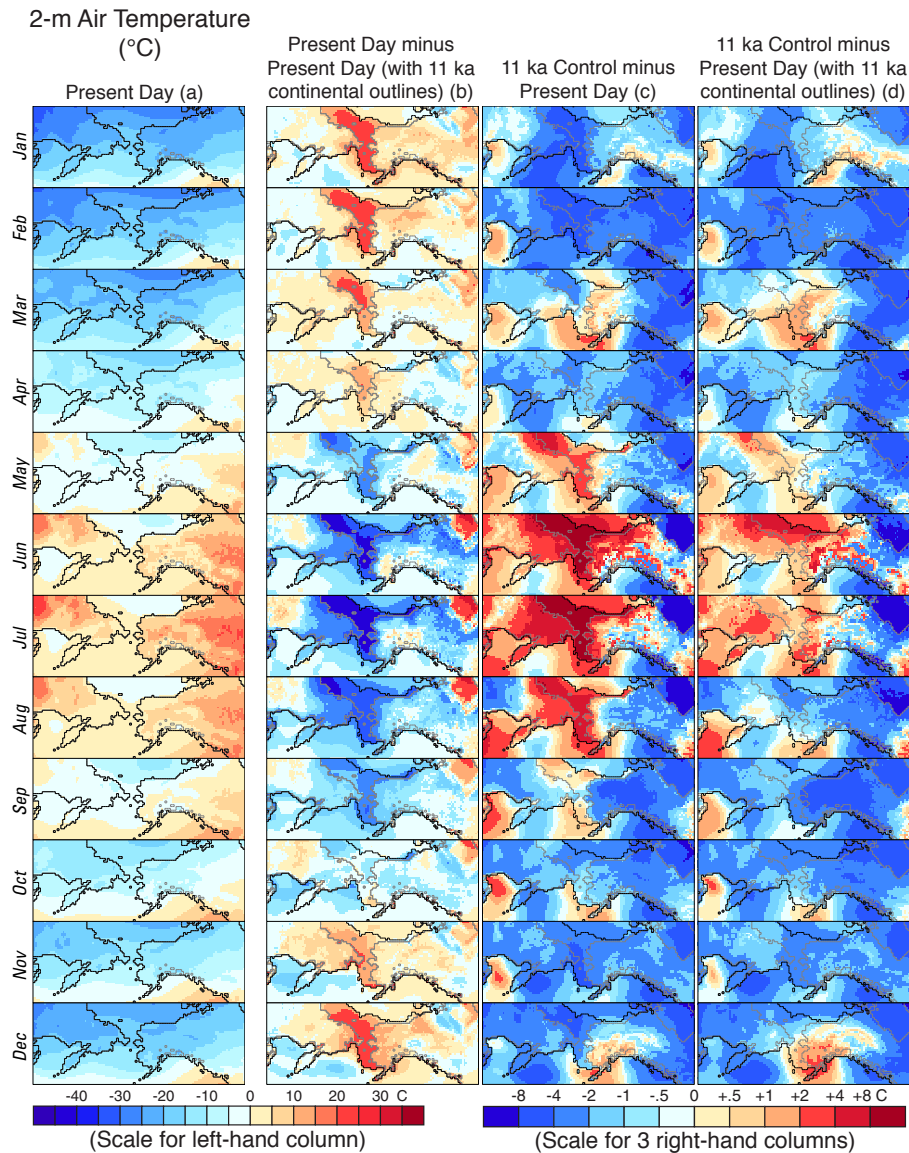


Figure 5. Simulated 2 m air temperature. **(a)** Present Day (0 ka) simulation; **(b)** effect of land-bridge flooding on present-day climatology (Present Day minus Present Day with 11 ka Continental Outlines); **(c)** difference between 11 ka Control and present (11 ka Control minus Present Day); **(d)** difference between 11 ka Control and present as a result of insolation and boundary conditions other than sea level (11 ka Control minus Present Day with 11 ka Continental Outlines). Ice-sheet and coastal outlines as in Fig. 4.

lies of sensible and latent heat fluxes parallel one another throughout the year; they generally track both air temperature and surface skin temperature (not shown). The anomalies are negative from June through August, when the negative temperature anomalies are at their greatest and temperature and vapor-pressure gradients are likely also negative.

Feedbacks among the surface temperature and energy-balance anomalies are reflected to a limited extent by atmospheric circulation and moisture variables (Fig. S3a). In the region of negative warm-season temperature anomalies, 500 hPa surface height anomalies are also negative, and sea-level pressure anomalies are positive, consistent with the neg-

ative temperature anomalies. While spatially variable, precipitation anomalies are generally negative in the “flooded” region and positive in other regions.

3.2 The 11 ka Control simulation and differences with the present

The 11 ka Control simulation is intended to portray the regional climate just before land-bridge flooding, vegetation change and thaw-lake development occurred (Fig. S4). This simulation forms the basis for the calculation of “experiment-minus-control” anomalies at 11 ka. The 11 ka Control simu-

lation also can be compared with present-day simulations to separate and quantify the effect of the “global”, as opposed to Beringia-specific, changes in boundary conditions: the former being insolation, greenhouse gas, ice sheet, and eustatic sea level, the latter being the state of the ocean shelves, land bridge and land surface (Fig. 5c; S5 and S6).

In the *11 ka Control* simulation, temperatures are generally lower than present during much of the year, reflecting the still substantial Northern Hemisphere ice sheets and slightly lower greenhouse gases relative to present (Fig. 5c). The radiative effects of the ice sheets and greenhouse gases are modulated by the greater amplitude of the annual cycle of insolation relative to present (Fig. 2). Overall, the amplitude of the annual cycle of temperature is greater than present. There is also a strong east–west gradient in temperature anomalies, which are strongly negative over and adjacent to the ice sheet. The insolation forcing is greatest from May–September and is maximally expressed in the May-through-August temperatures, when the strongest positive anomalies over the emergent land bridge occur (Fig. S5a).

The combination of the annual forcing, attributed to the ice sheets, lowered sea level, lower greenhouse gas concentrations, and the seasonally varying insolation forcing is registered by large spatial variations in the anomalies of the energy-balance components. In general, the sign of the anomalies is opposite to those discussed in the land-bridge flooding section (Sect. 3.1) because the sense of the continental-outline changes is reversed in this experiment (i.e., here the anomalies are calculated as *11 ka Control* with the 11 ka continental outline minus the *Present Day* simulation, whereas in Sect. 3.1 the anomalies are calculated as *Present Day* minus *Present Day with 11 ka Continental Outlines*). Further contributions to the spatial patterns of the anomalies are attributed to the ice sheet, which, in summer, is characterized by strongly negative anomalies in net shortwave radiation, net radiation, and sensible and latent heat fluxes, and strongly positive anomalies in net longwave radiation and substrate heat flux (Fig. S5). Atmospheric circulation and the attendant moisture anomalies are determined mainly by the hemispheric circulation, which is influenced by the 11 ka ice sheet (Bartlein et al., 2014). Precipitation anomalies generally follow those of temperature, and as a consequence, soil-moisture anomalies are generally negative, especially near the ice sheet from November through July (Fig. S5). Exceptions to this pattern occur in western Beringia and in the interior of eastern Beringia in summer.

Both the (exposed) land bridge and the 11 ka insolation enhance seasonality at 11 ka. Differencing the *11 ka Control* and the *Present Day with 11 ka Continental Outlines* simulations (Fig. 5d; S6) removes the effect of land-bridge flooding and highlights the effects of 11 ka insolation and the 11 ka ice sheet. The ice sheet exerts a general cooling effect year-round, and during the short summer season enhanced insolation results in air temperatures that are higher than those of present. Thus, at 11 ka, the presence of the land bridge

amplifies the insolation forcing and is an important driver of higher seasonality and relatively warm summers compared with present.

3.3 The 11 ka experiments

3.3.1 Sea level

The impact of land-bridge flooding at 11 ka is illustrated by the *11 ka Sea-Level* simulation. Figure 6 shows the relationship between net radiation and temperature when the land bridge is flooded (January and July anomalies for contrast). The major influence on the energy balance comes from changing land to water, but the effects are not spatially uniform, as is the case for the present-day land-bridge flooding experiment (Sect. 3.1). In Beringia, winter insolation is extremely low, and the January radiation balance is dominated by longwave radiation: incoming longwave radiation is relatively constant but can be affected by circulation both within the RCM domain and through hemispheric circulation in the GCM, while outgoing longwave radiation is dependent upon surface properties and their respective temperatures, which here drive most of the observed variation. January net radiation anomalies show a strong dipole: positive north of Siberia (Laptev Sea) and negative over the land bridge (Fig. 6). This pattern results from changing the present-day shelf north of Siberia from land to sea ice, which consequently has low surface temperatures throughout the year. An examination of other simulated variables indicates that this change results in decreased upward longwave radiation but little change in downward longwave radiation, and hence the mean difference in net radiation is positive. In contrast, in the ocean directly north and south of the Bering Strait (Chukchi and Bering Seas), sea ice is present seasonally. In January the ice is not yet at its maximum thickness for the year so there is upward energy flux (greater upward longwave radiation). The difference in mean net radiation is negative, and thus surface temperature is relatively higher (see also Fig. S8b).

The net radiation dipole is absent in July (Fig. 6). While sea ice in the Chukchi and Bering Seas melts, the seasonal variation in temperature is strongly lagged. Even in July there is some sea ice present, and temperatures are cooler than they would be otherwise owing to its relatively high albedo. The ocean warms in late summer and fall as the ice reaches minimum extent, leading to the warmer January conditions described above. Overall, summer temperatures in the vicinity of the flooded land bridge are cooler than when the land bridge is in place.

3.3.2 Vegetation

The effects of changing vegetation from low tundra to a tundra–woodland mosaic on both sides of the land bridge produces modest warming with the clearest effect in May (Fig. 7). While upward longwave radiation is relatively high, net downward shortwave radiation is greater, a response to

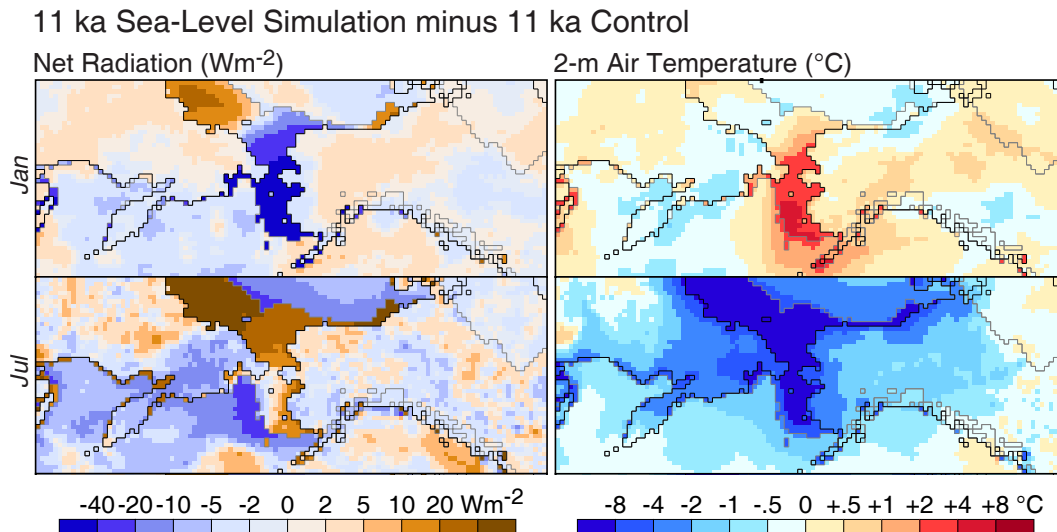


Figure 6. Results of 11 ka Sea Level experiment. Panels show the effect of flooding the land bridge at 11 ka (11 ka Sea Level minus 11 ka Control). Net radiation (left) and 2 m air temperature (right) for January (upper) and July (lower). Strong winter warming and summer cooling is seen over areas of flooded ocean shelf and adjacent land areas. Ice-sheet and coastal outlines as in Fig. 4.

the lowered albedo of the wooded land surface, which leads to a positive net radiation balance. In May, an air temperature increase of 1–3 $^{\circ}\text{C}$ (relative to the 11 ka Control simulation) is simulated over wooded areas, reflecting increases in sensible and latent heat fluxes. Substrate heat flux is lower as the land–atmosphere temperature gradient is reduced (Fig. S10b).

In winter (January) net radiation anomalies due to changed vegetation are small (Fig. 7). In tundra areas winter temperatures are slightly but consistently colder, reflecting less overall flow of heat to the ground and hence less upward longwave radiation in winter.

3.3.3 Lakes

Although the overall effect of placing lakes on the landscape is modest, it produces a clear pattern in summer (e.g., July; Fig. 8 top, S11 and S12), when grid cells occupied by lakes are cooler than surrounding areas or than in the 11 ka Control simulation. For western Alaska, latent heat-flux anomalies are positive in June, while net radiation and sensible heat-flux anomalies are positive in June and July, and generally 0 or negative the rest of the year (Fig. 8). For the entire study domain, the surface-temperature differences between the 11 ka Lakes simulation and the 11 ka Control simulation are substantial during April–August, and the accompanying changes in atmospheric circulation are consistent with these differences (Fig. 8, S12). Positive sea-level pressure or 500 hPa height anomalies (e.g., April) reflect greater heating at the surface and consequent displacement of the circulation, whereas the negative anomalies (e.g., July) reflect atmospheric cooling and subsequently lower and displaced 500 hPa height-anomaly patterns, particularly over the

southern-central part of the land bridge where there are additional interactions with SSTs (Fig. S12). The overall impact of thaw-lake formation relative to that of vegetation is still small, however, and similar to that noted for “column-mode” simulations with an RCM under present-day conditions (Rivers and Lynch, 2004).

3.3.4 All

The 11 ka All simulation shows the combined impact of all three land-cover changes (land-bridge flooding, vegetation change and thaw-lake formation). Figure 9 compares the monthly mean 2 m air temperature anomalies for changed vegetation, changed sea level and all land-cover features changed together at 11 ka (see also Fig. S14). The vegetation change at 11 ka (Fig. 9a) acts to amplify the insolation effect, making the whole year warmer, especially in spring and early summer (April through June), when there is greater absorption of incoming shortwave radiation relative to other times of the year or to the same time of year in the 11 ka Control simulation. This increased absorption leads to more heat storage in late summer, which carries over and is released during the winter season, thereby increasing upward longwave radiation and causing a slight warming.

Changing sea level has the largest effect (Fig. 9b). In winter the temperature anomaly is largely controlled by land-bridge flooding. Because there is minimal incoming shortwave radiation in winter (see above), the observed changes are modulated by albedo differences. The vegetation effect is overwhelmed by the sea-level effect through much of the year; it is only strongly expressed from April to June in the continental areas (Fig. 9c). The sea-level change acts to make

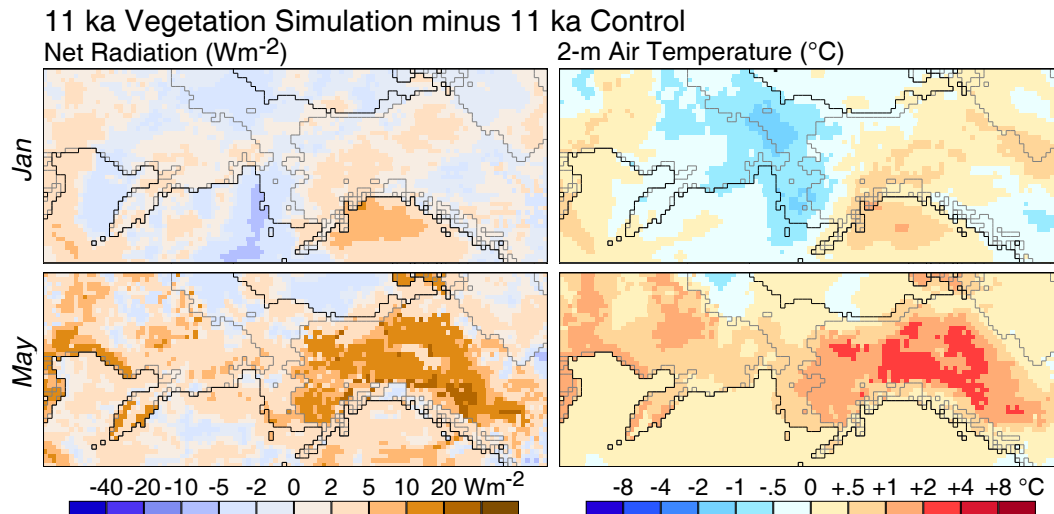


Figure 7. Results of *11 ka Vegetation* experiment (*11 ka Vegetation* minus *11 ka Control*). Panels show net radiation (left) and 2 m air temperature (right) for January (upper) and May (lower). The effect of taller, denser shrub/tree cover is seen most strongly in May, when 2 m air temperatures increase by 1–3 °C over the control values. Ice-sheet and coastal outlines as in Fig. 4.

winters warmer and summers cooler, countering the amplification of seasonality due to 11 ka insolation.

3.4 Principal responses other than temperature and energy-balance variables: *11 ka Control* and *11 ka All vs. Present Day*

During the interval from the LGM to present, the principal changes over the North Pacific and adjacent land areas in atmospheric circulation and variables that depend on circulation (i.e., clouds and precipitation) were governed largely by the retreat of the North American ice sheets, with secondary influences from land–ocean temperature contrasts induced by insolation variations and ocean heat transport (Bartlein et al., 2014). In particular, when large, the ice sheets in GENESIS perturbed the upper-level winds, generating a “wave-number-1” (one circumpolar ridge-and-trough) pattern that resulted in stronger-than-present southerly flow over Beringia, while at the surface, a strong glacial anticyclone developed. This circulation pattern results in the simulation of LGM near-surface air temperatures across much of the region that were as warm as or warmer than present. By 11 ka, these effects had greatly attenuated, but large-scale effects on Northern Hemisphere circulation caused by the remnant ice sheet and greater land–ocean temperature contrasts in summer are apparent in the AGCM simulations that provide the lateral boundary conditions for the RCM. As a consequence, relatively modest regional-scale modifications of the large-scale circulation might be expected in the different 11 ka RCM experiments. However, given the topographic complexity of the region even small changes in circulation could have large consequences on clouds, precipitation and soil moisture (although soil moisture is also governed by

surface water- and energy-balance variables; Edwards et al., 2001). In Beringia, at 11 ka as at present, below-freezing cold season temperatures constrain intra-annual variations in soil moisture. As a consequence, January soil-moisture anomalies are related more to late summer and early autumn atmospheric circulation and moisture conditions than they are to contemporaneous wintertime conditions.

The impact of larger-scale circulation anomalies represented in the GCM can be seen in RCM simulations for Beringia (Fig. 10; also see Supplement figures). The anomalies with respect to the present day differ little between the *11 ka Control* and *11 ka All* simulations (Fig. 10a and b), and consequently can be discussed together. The anomalies also indicate that effects of the land-cover changes on regional circulation were small. In the 11 ka simulations, January 500 hPa heights are generally lower than present across the North Pacific and higher than present over the southeastern part of the domain, while at the surface, negative sea-level pressure anomalies are centered over southwest Alaska and the Aleutian Islands. This pattern is somewhat analogous to the “January Northeast Pacific negative” pattern of Mock et al. (1998). As a consequence of the stronger-than-present southeasterly flow into eastern Beringia both at the surface and in the upper atmosphere, cloudiness and precipitation are greater than present in southern Alaska. In eastern Siberia, stronger-than-present offshore flow creates drier-than-present conditions. Soil-moisture anomalies show a strong east (dry) to west (wet) pattern, which develops in October and persists through April.

In July, an east–west contrast in 500 hPa height anomalies exists (Fig. 10). Positive anomalies occur in the western part of the region, where at present the East Asian trough prevails, while negative anomalies occur over east-

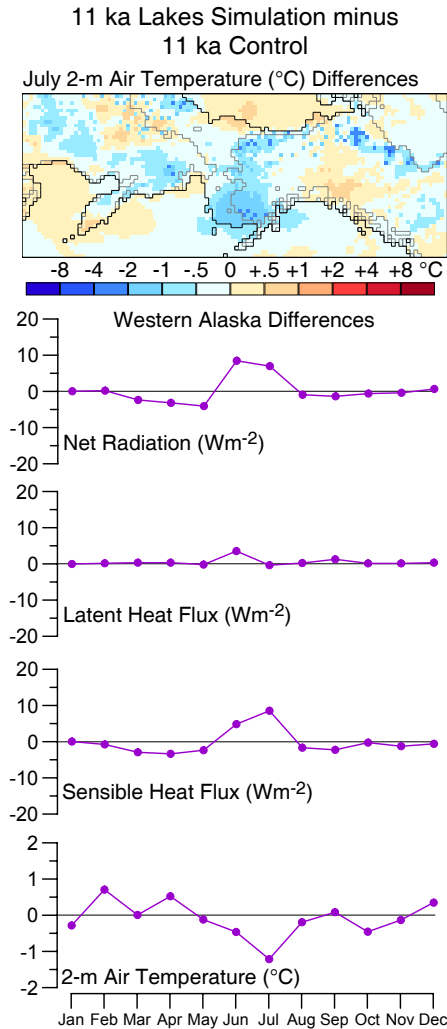


Figure 8. Results of *11 ka Lakes* experiment. Top panel shows July 2 m air temperature differences (*11 ka Lakes* minus *11 ka Control*). Lower panels show mean monthly differences for energy fluxes and temperature for RegCM grid cells in western Alaska (170–150° W longitude), where cooling is most pronounced. Ice-sheet and coastal outlines as in Fig. 4.

ern Beringia, where at present a semipermanent ridge develops. This anomaly pattern produces stronger-than-present zonal flow over the region, which is consistent with (i) the continued presence of negative (relative to present) 500 hPa height and sea-level pressure anomalies over the Arctic Basin upstream of the ice sheet and (ii) the developing enhancement of the North Pacific subtropical high (Bartlein et al., 2014). As a consequence of the stronger-than-present zonal flow, coastal areas in the southeastern quadrant of the region feature stronger-than-present onshore flow, and greater-than-present cloudiness and precipitation. In the interior of North America, precipitation is lower than present, which is reflected by July soil-moisture anomalies. Soil-moisture anomalies have a broad-scale pattern with generally positive

values in western Beringia and negative values in eastern Beringia, a first-order effect of a similar general pattern of precipitation anomalies (Figs. S5 and S15).

The 11 ka land-surface changes, which are dominated year-round by the land-bridge flooding and in spring in eastern Beringia by vegetation changes, have only a modest impact on atmospheric circulation and related variables, particularly in winter (Fig. 10c). In July, the large negative temperature anomaly centered over the flooded region (Fig. 9c) is accompanied by a broad negative 500 hPa height anomaly (Fig. 10c). At the surface a weak dipole prevails, with negative sea-level pressure anomalies over the Bering Sea contrasting with positive anomalies over the Arctic Basin. This pattern results in stronger-than-present upper-level flow into southwestern Alaska, wetter-than-present conditions, and positive soil-moisture anomalies, which appear in an arc from Kamchatka to southwestern Alaska. In the west, the circulation anomalies reinforce a general pattern of greater-than-present soil moisture, while in southwest Alaska the moister conditions (Fig. 10c, S14) reverse the sign of negative 11 ka minus present anomalies. Overall, within-region changes in atmospheric circulation related to the various land-cover changes appear less important than changes in the surface energy balance and temperature in determining the nature of the early Holocene climate.

3.5 Comparison of simulated temperatures for *11 ka Control*, *11 ka All*, *6 ka* and *Present Day*

The general trends in the climate of Beringia over the Holocene can be described with the help of the *6 ka* simulation, in which the only difference in boundary conditions relative to present is the insolation forcing. Thus, the impact of insolation can be isolated, which is not feasible at 11 ka due to the amplifying or offsetting effects of the land-cover changes. Figure 11 shows monthly averages of simulated temperature for 11 ka prior to land-cover changes (*11 ka Control*), 11 ka with land-cover changes (*11 ka All*), *6 ka* (with 6 ka insolation, no ice sheet and modern vegetation) and *Present Day* (0 ka). The changing pattern of yearly insolation (Fig. 2) can be seen in the longer period of above-freezing temperatures at 6 ka and present: the progressively later occurrence during the Holocene of the summer insolation-anomaly maximum gradually extends summer into autumn.

Both the *11 ka Control* and *11 ka All* simulations are affected by the presence of the LIS and CIS and their attendant zonal cooling effect, which counters the insolation and land-bridge effects. With no land-cover change (e.g., the *11 ka Control* simulation; Fig. 11a), the land bridge is relatively warm in summer. However, eastern Beringia, which includes the western edge of the LIS, is cooler than Siberia, which has no ice sheet (see also Figs. S5 and S15). The coolest summer is seen in the *11 ka All* simulation with land-cover changes

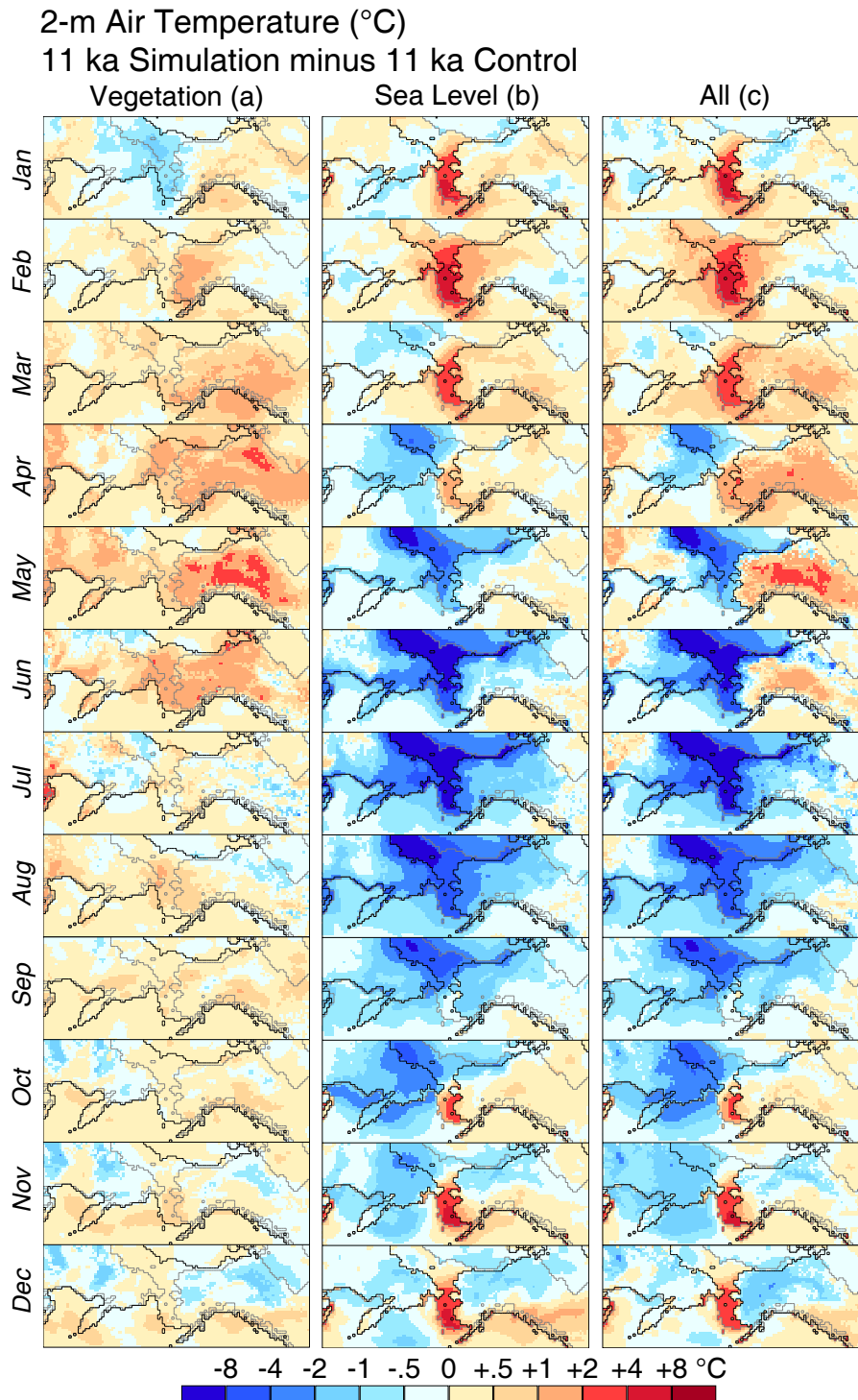


Figure 9. The effect on 2 m air temperature (°C) of changing vegetation (a), sea level (b) and all three land cover changes (vegetation, sea level and lakes; c) at 11 ka. Ice-sheet and coastal outlines as in Fig. 4.

(Fig. 11b), when the warming effect of the land bridge in summer is removed.

From 11 to 6 ka, all of the boundary conditions except insolation approached their present-day values. The insolation

anomaly at 6 ka (Fig. 2) reached its maximum in July (vs. in June at 11 ka) and anomalies were slightly greater than those at 11 ka in late summer and autumn (August through October). Relative to the 11 ka All simulation, air temperatures

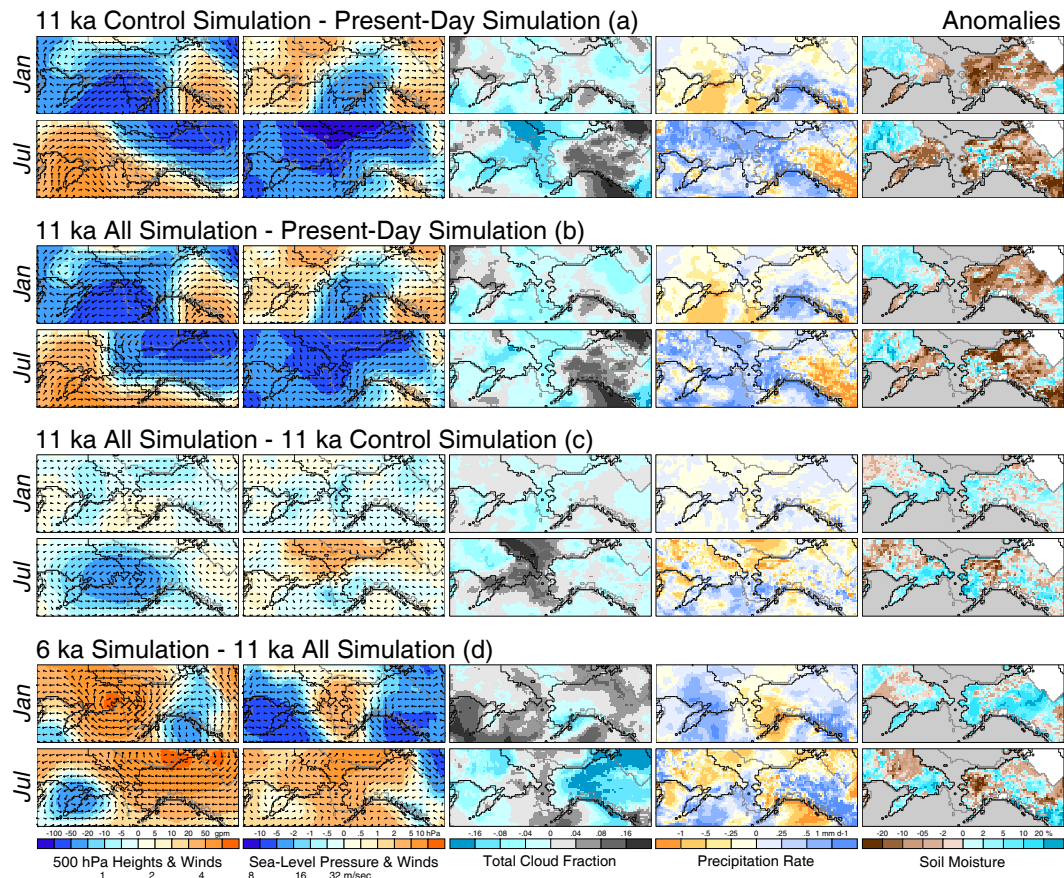


Figure 10. Atmospheric circulation (500 hPa heights and winds, sea-level pressure and surface winds), clouds, precipitation and soil-moisture anomalies. **(a)** 11 ka Control minus Present Day; **(b)** 11 ka All minus Present Day; **(c)** 11 ka All minus 11 ka Control; **(d)** 6 ka minus 11 ka All (showing the change between 11 and 6 ka). Ice-sheet and coastal outlines as in Fig. 4.

were generally higher across the region at 6 ka, particularly in the area that was ice-covered at 11 ka.

In many respects 6 ka is similar to present, but the continental heating that reflects the positive summer insolation anomaly at 6 ka is obvious, particularly in eastern Beringia (Fig. 11c). August and September are warmer at 6 ka than at 11 ka and also than at 0 ka (Fig. 11d). The cooling effect of the flooded land bridge is evident in adjacent land areas; in continental interiors, the effect is less strong, and the widespread presence of needleleaf forest may enhance summer warming via an albedo effect at both 6 and 0 ka (Fig. 4a).

The effect of changes in boundary conditions other than insolation can be isolated by considering anomalies and differences in February and August. The nature of the insolation variations are such that anomalies in both insolation amount and month length are nearly the same during those months at 11 and 6 ka (Fig. 2). Figure 12 shows the anomalies of net shortwave radiation, net radiation and temperature for February and August at 11 and 6 ka compared with present (Fig. 12a and c) and the change between 11 and 6 ka (Fig. 12b). As expected, the anomalies for shortwave radi-

ation in February are small, owing to low inputs at the top of the atmosphere in winter. The anomalies of net radiation for the 11 ka All simulation are quite spatially variable for reasons discussed in Sect. 3.3, while those of temperature are almost uniformly negative across the region. From 11 to 6 ka, net shortwave radiation in August increased substantially. Because insolation at the top of the atmosphere was similar in August at 11 and 6 ka (Fig. 2), the net shortwave increase was likely generated by changes in albedo and a general reduction in cloudiness over the region related to the expansion of the North Pacific subtropical high in summer (Fig. 10d), both consequences of the generally warmer conditions at 6 ka relative to earlier. The general reversal in sign of the August net radiation and temperature anomalies between 11 and 6 ka (Fig. 12a vs. c) is thus related to boundary-condition changes and mechanisms internal to the climate system, as distinct from changes in August insolation levels; these changes include an increase in greenhouse gas levels, the final disappearance of the ice sheet and continued changes in land-surface cover.

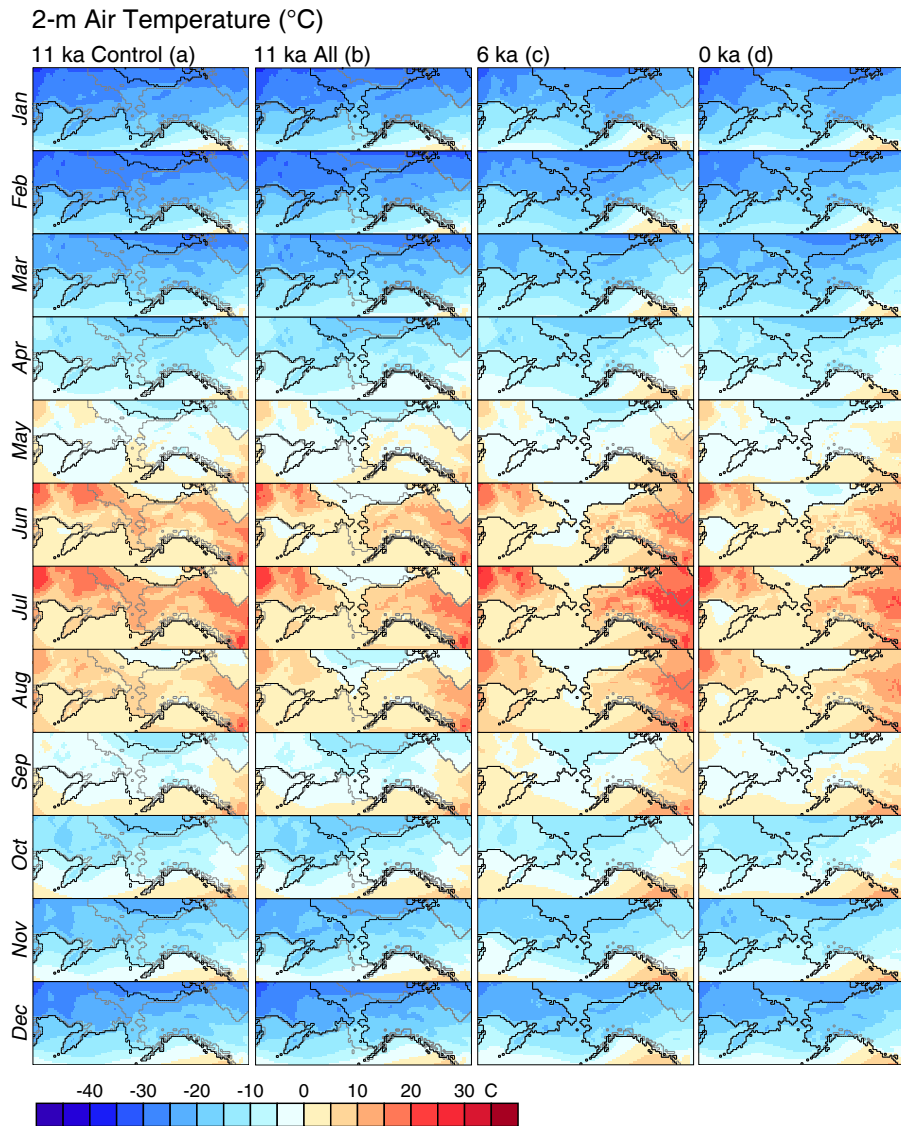


Figure 11. Monthly mean simulated temperature for 11 ka Control (a), 11 ka with changed surface properties (11 ka All; b), 6 ka (c), and present (0 ka; d). Ice-sheet and coastal outlines as in Fig. 4.

4 Discussion

4.1 Major features of the 11 ka simulated climate

In the 11 ka All simulation the annual cycle of temperature in Beringia is highly seasonal, with warmer summers and colder winters than present (Fig. S15b). The summer and shoulder seasons are short and shifted earlier in the seasonal cycle, with warming limited to 3 months (May–July). Thaw lakes and wetlands produce modest and localized cooling in summer and warming in winter (Fig. 8). The vegetation change from tundra to deciduous tall shrub and/or woodland produces a widespread warming in spring and early summer greater than that induced by the 11 ka insolation regime (Fig. 7). In contrast, the land-bridge flooding produces gen-

erally cooler conditions in summer but warmer conditions in winter that are manifested mainly on the flooded shelves and in eastern Beringia (Fig. 6). Precipitation anomalies are generally small and spatially heterogeneous, but precipitation in summer is generally lower than at present in eastern Beringia (Fig. 10b), as is soil moisture.

It is reasonable that the insolation anomaly at 11 ka had a major effect on summer temperature maxima and seasonality. Beringia was adjacent to the LIS, and while this likely had a moderating influence on temperature maxima, at least in regions proximal to the ice (Bartlein et al., 1991), a range of proxy records support a terrestrial thermal maximum in the earliest Holocene (e.g., Ritchie et al., 1983; Kaufman et al., 2004). In the 11 ka All simulation, positive net radiation

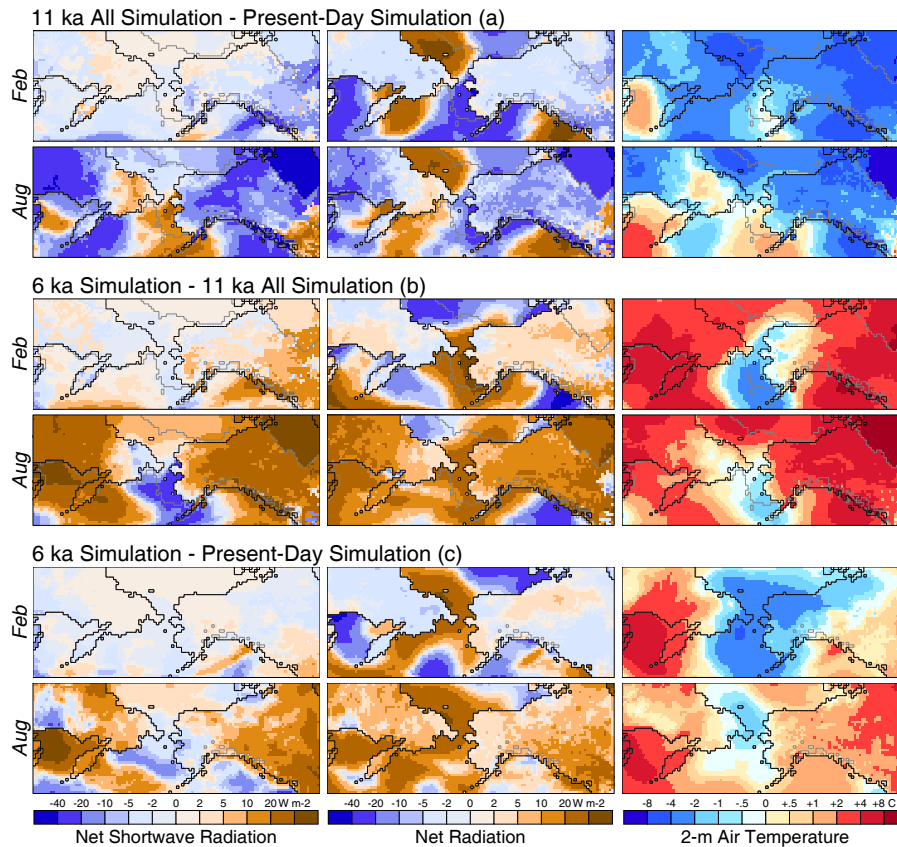


Figure 12. Net shortwave radiation (surface), net radiation and 2 m air temperature differences for February and August. **(a)** 11 ka All minus Present Day, illustrating the impact of 11 ka insolation (relative to that at present); **(b)** 6 ka minus 11 ka All, illustrating the impact of changes in boundary conditions other than concurrent insolation between 11 and 6 ka; **(c)** 6 ka minus Present Day, illustrating the impact of 6 ka insolation (relative to that at present). Ice-sheet and coastal outlines as in Fig. 4.

anomalies are linked to positive summer temperature anomalies of 1.0 to $>4.0^{\circ}\text{C}$ over much of the Beringian land mass in June and July, and much of Siberia is warmer in May (Fig. S15b). The summer, however, is short compared with today (Fig. 2), temperatures in August and September are cooler than present, and winters are colder than present.

The simulations show lower summer precipitation and stronger summer heating (relative to present) and large negative soil-moisture anomalies in much of Beringia, particularly eastern Beringia. Low summer precipitation at 11 ka in the interior of Alaska and Yukon is also supported by observations of relatively low lake levels until ~ 10 ka (Abbott et al., 2000; Barber and Finney, 2000; Anderson et al., 2005; Finney et al., 2012). Stand modeling (Chapin and Starfield, 1997) and empirical observation (Barber et al., 2000) indicate that warm, dry conditions favor hardwoods and reduce the growth of evergreen conifers. In addition, long, cold winters, short shoulder seasons and winter soil-moisture deficits (resulting from late summer and early autumn atmospheric and moisture conditions; see Sect. 3.4) may have combined to generate physiological drought going into spring, which

would also favor the woody deciduous growth forms observed in the paleorecord (Fig. 3a).

4.2 Key responses and feedbacks to 11 ka land-cover changes

The 11 ka set of experiments explores the sensitivity of the regional climate to land-surface changes brought about as a consequence of deglacial warming.

4.2.1 Flooding the land bridge

The land-bridge transgression is often cited as a key factor affecting early-Holocene Beringia (e.g., Burn, 1997; Abbott et al., 2000; Mann et al., 2001). In the 11 ka land-bridge flooding experiment (*11 ka Sea Level*) summer and autumn temperatures across Beringia are greatly reduced, whereas winter temperatures increase (Fig. 6). This is the largest single response of regional climate to a land-cover change. The change works in opposition to the insolation forcing, driving the system towards weaker seasonality and cooler summers. The changes are seen particularly in eastern Beringia,

downwind of the land–sea reconfiguration. Our results emphasize the influence of the land-bridge transgression, but because we conducted a single sensitivity experiment, as opposed to a sequence of simulations, the results cannot clarify a more detailed temporal pattern of change. However, the shift in seasonality and growing-season temperature and moisture may have promoted landscape hydrologic changes such as paludification (Jones and Yu, 2010) and increasing lake levels (Abbott et al., 2000; Barber and Finney, 2000), particularly across eastern Beringia.

4.2.2 Vegetation feedbacks

The main response of replacing tundra with deciduous tall shrub and/or woodland is seen in the net radiation and temperature values for spring and early summer, when snow is still present (Fig. 7, S10b). The lower albedo of the woodland cover leads to stronger heating, particularly in the eastern region. A positive feedback is set up via the establishment of taller-stature vegetation, which contributes to a warmer spring and works in opposition to the spring cooling (Fig. 5c) that is a result of the land-bridge flooding plus the global controls of lower-than-present atmospheric greenhouse gas concentrations and SSTs.

4.2.3 Thaw lakes

Conversion of portions of the land surface to shallow lakes via thermokarst processes would be expected to influence surface energy dynamics. Rivers and Lynch (2004) demonstrated a moderate response in column model experiments for single locations in Beringia. In our study, the inclusion of thaw lakes shows a small local effect that becomes undetectable at larger spatial scales. These results align with those of studies examining lake effects on modern climate in a GCM (Subin et al., 2012). Regionally, radiation and heat-flux anomalies are small (within inherent model variability) and spatially incoherent, suggesting that there is no regional impact of the lakes on climate via surface energy exchanges (Fig. 8). However, thaw lakes and peatlands are sources of greenhouse gas flux to the atmosphere (Walter et al., 2006; MacDonald et al., 2006; Walter Anthony et al., 2014), and their initiation and spread ca. 14–10 ka may have had an impact on global climate through enhanced gas emissions.

4.2.4 All changes combined

Atmospheric circulation changes in Beringia related to the joint effect of the land-surface changes are small despite large changes in the surface energy balance and temperature (Fig. 10c). When the sea level, vegetation and lake changes are combined, the vegetation effect, especially in eastern Beringia, opposes cooling brought about by the land-bridge transgression to make land temperatures slightly warmer in spring and early summer (Fig. 9c). However, the regional cir-

ulation is largely dominated by hemispheric-scale circulation changes. For example, at 11 ka, the larger-scale circulation leads to contrasts in precipitation and soil moisture between western (wetter than present) and eastern (drier than present) Beringia (Fig. 10b, S15). This result may explain the late (ca. 13 ka) filling and low levels of shallow (i.e., < 15 m) lakes in the easternmost part of Beringia (Abbott et al., 2000; Barber and Finney, 2000) compared with similar lakes in western Alaska and Siberia, which were at least partially full before 13 ka and even during the last glacial maximum (Abbott et al., 2010; Ager, 2003; Lozhkin et al., 1993).

4.3 Comparison of 11, 6 ka and present day

The simulated temperature patterns for the three time periods (Fig. 11) show the effect of the precession of the equinoxes in lengthening the summer season and in the progression to a later summer temperature maximum with time. Increased warmth in summer at 11 ka (Fig. 11a) is reduced with all land-cover changes in place, particularly in the area of the land bridge (Fig. 11b). In interior continental regions, the absence of the ice sheet at 6 ka, combined with higher-than-present summer insolation and widespread cover of needle-leaf forest, leads to temperatures as warm, or warmer than, those seen at 11 ka (Fig. 11c). Thus, the 11 ka thermal maximum was manifest as a short, intense summer period with relatively low effective moisture, whereas summers warmer than present continued until at least 6 ka, with more moisture and a lengthening growing period. As these changes developed from 11 to 6 ka, they would have been major drivers of a range of terrestrial responses, such as further shifts towards evergreen forest dominance (Anderson et al., 2004), permafrost changes and the spread of paludification (Jones and Yu, 2010) and hydrological changes (e.g., increasing lake levels; Edwards et al., 2000b; Abbott et al., 2000).

4.4 Broader implications

Our modeling experiments clearly demonstrate how the regional climate response to global forcing can be amplified, attenuated or reversed by the regional controls. Beringian climate was subject to a range of controls that waxed and waned, generating a series of unique climate states through the mid-Holocene. The subtlety and heterogeneity of response to forcing combinations may explain anomalous or conflicting paleodata. For example, the subtle (even absent) expression of the Younger Dryas event over much of the region (Kokorowski et al., 2008) is consistent with the initial dominance of insolation and subsequently the effect of the progressive land-bridge transgression (beginning at ~ 13 ka) on Beringian climate, both of which might have masked the Younger Dryas cooling. The spatial heterogeneity of summer warmth and its different seasonal expression through time argues against defining a single thermal maximum for the Holocene, even within Beringia (cf. Kaufman et al., 2004), as

this may unnecessarily constrain views of how Beringian climate evolved and overemphasize the importance of the early Holocene as a period of extreme warmth.

Furthermore, the results of the model experiments have a range of implications not only for interpretations of past Beringian environments but also for the study of future climate change in northern regions through our identification of regionally relevant mechanisms and feedbacks. For example, attention is currently focused on the potential effects of future climate change in arctic regions, including increased shrub size and the northward expansion of woody vegetation cover, both shrubs and boreal forest. Our results indicate that vegetation changes from low shrub tundra to tall shrubs or deciduous woodland can increase spring temperatures, in general agreement with other studies examining the effects of potential future vegetation change in the Arctic (e.g., Swann et al., 2010; Bonfils et al., 2012). The effect appears to be robust, even under markedly different conditions of insolation and seasonality.

The study of Earth-system responses to climate change both past and present, such as the modeling of carbon balance, hydrology, and permafrost dynamics, requires a foundation of adequate regional climate detail to produce coherent results. Our regional modeling study demonstrates the complexity of the interaction of hemispheric and regional controls and may serve as a basis for further investigations of key elements of Holocene ecosystem dynamics in Beringia.

The Supplement related to this article is available online at doi:10.5194/cp-11-1197-2015-supplement.

Author contributions. P. J. Bartlein developed the study concept; P. J. Bartlein, M. E. Edwards, L. B. Brubaker, P. M. Anderson, A. V. Lozhkin and S. W. Hostetler created the input data for the simulations; S. W. Hostetler produced the climate model simulations; P. J. Bartlein created the resultant climate maps; P. J. Bartlein, M. E. Edwards, S. W. Hostetler, and S. L. Shafer analyzed the results; P. J. Bartlein, M. E. Edwards, and S. L. Shafer wrote the first draft of the manuscript and all authors contributed to the final draft.

Acknowledgements. We thank Jay Alder and Nancy Bigelow for their comments on the manuscript and Richard Pellier for his assistance with figures. Funding for this research was provided by NSF Grants ATM-0001643 to P. J. Bartlein, OPP-001874 to P. M. Anderson and L. B. Brubaker, OPP-0218785 to M. E. Edwards, and grants from the Far East Branch of the Russian Academy of Sciences (12-III-A-09-198; 12-II-CO-08-024; 15-I-2-067) and Russian Foundation for Fundamental Research (15-05-06420; 14-05-00573) to A. V. Lozhkin. S. W. Hostetler was supported by the U.S. Geological Survey (USGS) National Research Program and S. W. Hostetler and S. L. Shafer were supported by the USGS Climate and Land Use Change Research and Development Program.

Any use of trade, firm, or product names is for descriptive purposes only and does not imply endorsement by the US Government.

Edited by: V. Rath

References

- Abbott, M. B., Finney, B. P., Edwards, M. E., and Kelts, K. R.: Lake-level reconstructions and paleohydrology of Birch Lake, central Alaska, based on seismic reflection profiles and core transects, *Quaternary Res.*, 53, 154–166, 2000.
- Abbott, M. B., Edwards, M. E., and Finney, B. P.: A 40 000-yr record of environmental change from Burial Lake in Northwest Alaska, *Quaternary Res.*, 74, 156–165, 2010.
- ACIA: Impact of a Warming Arctic: Arctic Climate Impact Assessment, Cambridge University Press, Cambridge, 1020 pp., 2004.
- Ager, T. A.: Late Quaternary vegetation and climate history of the central Bering land bridge from St. Michael Island, western Alaska, *Quaternary Res.*, 60, 19–32, 2003.
- Ager, T. A. and Phillips, R. L.: Pollen evidence for Late Pleistocene Bering land bridge environments from Norton Sound, Northeastern Bering Sea, Alaska, *Arct. Antarct. Alp. Res.*, 40, 451–461, 2008.
- Alder, J. R. and Hostetler, S. W.: Global climate simulations at 3000-year intervals for the last 21 000 years with the GEN-MOM coupled atmosphere-ocean model, *Clim. Past*, 11, 449–471, doi:10.5194/cp-11-449-2015, 2015.
- Anderson, L., Abbott, M. B., Finney, B. P., and Edwards, M. E.: Palaeohydrology of the Southwest Yukon Territory, Canada, based on multiproxy analyses of lake sediment cores from a depth transect, *Holocene*, 15, 1172–1183, 2005.
- Anderson, P. M., Edwards, M. E., and Brubaker, L. B.: Results and paleoclimate implications of 35 years of paleoecological research in Alaska, in: *The Quaternary Period in the United States, Developments in Quaternary Science*, edited by: Gillespie, A. E., Porter, S. C., and Atwater, B. F., Elsevier, New York, 427–440, 2004.
- Barber, V. A. and Finney, B. P.: Late Quaternary paleoclimatic reconstructions for interior Alaska based on paleolake-level data and hydrologic models, *J. Paleolimnol.*, 24, 29–41, 2000.
- Barber, V. A., Juday, G. P., and Finney, B. P.: Reduced growth in Alaskan white spruce from 20th century temperature-induced drought stress, *Nature*, 405, 668–673, 2000.
- Bartlein, P. J., Anderson, P. M., Edwards, M. E., and McDowell, P. M.: A framework for interpreting paleoclimatic variations in eastern Beringia, *Quatern. Int.*, 10–12, 73–83, 1991.
- Bartlein, P. J., Hostetler, S. W., and Alder, J. R.: Paleoclimate, in: *Climate Change in North America, Regional Climate Studies*, edited by: Ohring, G., Springer, 1–51, doi:10.1007/978-3-319-03768-4_1, 2014.
- Berger, A. L.: Long-term variations of daily insolation and Quaternary climatic changes, *J. Atmos. Sci.*, 35, 2362–2367, 1978.
- Bigelow, N. H., Brubaker, L. B., Edwards, M. E., Harrison, S. P., Prentice, I. C., Anderson, P. M., Andreev, A. A., Bartlein, P. J., Christensen, T. R., Cramer, W., Kaplan, J. O., Lozhkin, A. V., Matveyeva, N. V., Murray, D. F., McGuire, A. D., Razzhivin, V. Y., Ritchie, J. C., Smith, B., Walker, D. A., Gajewski, K., Wolf, V., Holmqvist, B. H., Igarashi, Y., Kremenetskii, K., Paus, A.,

- Pisarcic, M. F. J., and Volkova, V. S.: Climate change and Arctic ecosystems: 1. Vegetation changes north of 55° N between the last glacial maximum, mid-Holocene, and present, *J. Geophys. Res.*, 108, 8170, doi:10.1029/2002JD002558, 2003.
- Binney, H. A., Willis, K. J., Edwards, M. E., Bhagwat, S. A., Anderson, P. M., Andreev, A. A., Blaauw, M., Damblon, F., Haesaerts, P., Kienast, F., Kremenetski, C. V., Krivonogov, S. K., Lozhkin, A. V., MacDonald, G. M., Novenko, E. Y., Oksanen, P., Sapelko, T. V., Valiranta, M., and Vazhenina, L.: The distribution of late-Quaternary woody taxa in northern Eurasia: evidence from a new macrofossil database, *Quaternary Sci. Rev.*, 8, 2445–2464, 2009.
- Bonan, G. B., Chapin III, F. S., and Thompson, S. L.: Boreal forest and tundra ecosystems as components of the climate system, *Climatic Change*, 29, 145–167, 1995.
- Bonfils, C. J. W., Phillips, T. J., Lawrence, D. M., Cameron-Smith, P., Riley, W. J., and Subin, Z. M.: On the influence of shrub height and expansion on northern high latitude climate, *Environ. Res. Lett.*, 7, 015503, doi:10.1088/1748-9326/7/1/015503, 2012.
- Burn, C. R.: Cryostratigraphy, paleogeography, and climate change during the early Holocene warm interval, western Arctic coast, Canada, *Can. J. Earth Sci.*, 34, 912–925, 1997.
- Chapin III, F. S. and Starfield, A. M.: Time lags and novel ecosystems in response to transient climatic change in Arctic Alaska, *Climatic Change*, 35, 449–461, 1997.
- Chapin III, F. S., Sturm, M., Serreze, M. C., McFadden, J. P., Key, J. R., Lloyd, A. H., McGuire, A. D., Rupp, T. S., Lynch, A. H., Schimel, J. P., Beringer, J., Chapman, W. L., Epstein, H. E., Euskirchen, E. S., Hinzman, L. D., Jia, G., Ping, C.-L., Tape, K. D., Thompson, C. D. C., Walker, D. A., and Welker, J. M.: Role of land-surface changes in Arctic summer warming, *Science*, 310, 657–660, 2005.
- Chase, T. N., Pielke, R. A., Kittel, T. G. F., Nemani, R., and Running, S. W.: Sensitivity of a general circulation model to global changes in leaf area index, *J. Geophys. Res.-Atmos.*, 101, 7393–7408, doi:10.1029/95JD02417, 1996.
- Collins, M., Knutti, R., Arblaster, J., Dufresne, J.-L., Fichetef, T., Friedlingstein, P., Gao, X., Gutowski, W. J., Johns, T., Krinner, G., Shongwe, M., Tebaldi, C., Weaver, A. J., and Wehner, M.: Long-term climate change: projections, commitments and irreversibility, in: *Climate Change 2013: The Physical Science Basis. Contribution of Working Group I to the Fifth Assessment Report of the Intergovernmental Panel on Climate Change*, edited by: Stocker, T. F., Qin, D., Plattner, G.-K., Tignor, M., Allen, S. K., Boschung, J., Nauels, A., Xia, Y., Bex, V., and Midgley, P. M., Cambridge University Press, Cambridge, UK, 1032 pp., 2013.
- Dorman, J. L. and Sellers, P. J.: A global climatology of albedo, roughness length, and stomatal resistance for atmospheric general circulation models as represented by the simple biosphere model (SiB), *J. Appl. Meteorol.*, 28, 833–855, 1989.
- Dyke, A. S., Moore, A., and Robertson, L.: Deglaciation of North America, *Geological Survey of Canada, Open File 1574*, 2003.
- Edwards, M. E., Anderson, P. M., Brubaker, L. B., Ager, T., Andreev, A. A., Bigelow, N. H., Cwynar, L. C., Eisner, W. R., Harrison, S. P., Hu, F.-S., Jolly, D., Lozhkin, A. V., MacDonald, G. M., Mock, C. J., Ritchie, J. C., Sher, A. V., Spear, R. W., Williams, J., and Yu, G.: Pollen-based biomes for Beringia 18 000, 6000 and 0 ¹⁴C yr BP, *J. Biogeogr.*, 27, 521–554, 2000a.
- Edwards, M. E., Bigelow, N. H., Finney, B. P., and Eisner, W. R.: Records of aquatic pollen and sediment properties as indicators of late-Quaternary Alaskan lake levels, *J. Paleolimnol.*, 24, 55–68, 2000b.
- Edwards, M. E., Mock, C. J., Finney, B. P., Barber, V. A., and Bartlein, P. J.: Modern-climate analogues for paleoclimatic variations in eastern interior Alaska during the past 14 000 years: atmospheric-circulation controls of regional temperature and moisture responses, *Quaternary Sci. Rev.*, 20, 189–202, 2001.
- Edwards, M. E., Brubaker, L. B., Lozhkin, A. V., and Anderson, P. M.: Structurally novel biomes: a response to past warming in Beringia, *Ecology*, 86, 1696–1703, 2005.
- Elias, S. A. and Brigham-Grette, J.: Late Pleistocene events in Beringia, in: *Encyclopedia of Quaternary Science*, 1057–1066, 2007.
- Elias, S. A., Short, S. K., and Birks, H. H.: Late Wisconsin environments of the Bering Land Bridge, *Palaeogeogr. Palaeoclimatol.*, 136, 293–308, 1997.
- Fairbanks, R. G.: A 17 000-year glacio-eustatic sea-level record – influence of glacial melting rates on the Younger Dryas event and deep-ocean circulation, *Nature*, 342, 637–642, 1989.
- Finney, B. P., Bigelow, N. H., Barber, V. A., and Edwards, M. E.: Holocene climate change and carbon cycling in a groundwater-fed, boreal forest lake: Dune Lake, Alaska, *J. Paleolimnol.*, 48, 43–54, 2012.
- Foley, J. A., Kutzbach, J. E., Coe, M. T., and Levis, S.: Feedbacks between climate and boreal forests during the Holocene, *Nature*, 371, 52–54, doi:10.1038/371052a0, 1994.
- Forbes, B. C., Fauria, M. M., and Zetterberg, P.: Russian Arctic warming and “greening” are closely tracked by tundra shrub willows, *Glob. Change Biol.*, 16, 1542–1554, 2010.
- Giorgi, F., Marinucci, M. R., and Bates, G. T.: Development of a second-generation regional climate model (RegCM2), Part I: Boundary-layer and radiative transfer processes, *Mon. Weath. Rev.*, 121, 2794–2813, 1993a.
- Giorgi, F., Marinucci, M. R., and Bates, G. T.: Development of a second-generation regional climate model (RegCM2), Part II: Convective processes and assimilation of lateral boundary conditions, *Mon. Weath. Rev.*, 121, 2814–2832, 1993b.
- Harvey, L. D. D.: On the role of high latitude ice, snow and vegetation feedbacks in the climatic response to external forcing changes, *Climatic Change*, 13, 191–224, 1988.
- Hill, P. R. and Solomon, S.: Geomorphologic and sedimentary evolution of a transgressive thermokarst coast, Mackenzie delta region, Canadian Beaufort Sea, *J. Coastal Res.*, 15, 1011–1029, 1999.
- Hopkins, D. M.: Thaw lakes and thaw sinks in the Imuruk Lake Area, Seward Peninsula, Alaska, *J. Geol.*, 57, 119–131, 1949.
- Hopkins, D. M.: Aspects of the paleogeography of Beringia during the late Pleistocene, in: *Paleoecology of Beringia*, edited by: Hopkins, D. M., Matthews, J. J. V., Schweger, C. E., and Young, S. B., Academic Press, New York, 127–150, 1982.
- Hostetler, S. W. and Bartlein, P. J.: Simulation of lake evaporation with application to modeling lake level variations of Harney-Malheur Lake, Oregon, *Water Resour. Res.*, 26, 2603–2612, 1990.
- Hostetler, S. W. and Bartlein, P. J.: Response of regional climate and surface processes in Western North America to a canonical Heinrich event, in: *Mechanism of Global Climate Change at Millennial Time Scales*, edited by: Clark, P. U., Webb, R. S., and Keig-

- win, L., AGU Monograph Series, American Geophysical Union, Washington, DC, 313–328, 1999.
- Hostetler, S. W., Giorgi, F., Bates, G. T., and Bartlein, P. J.: Lake–atmosphere feedbacks associated with paleolakes Bonneville and Lahontan, *Science*, 263, 665–668, 1994.
- Hostetler, S. W., Bartlein, P. J., Clark, P. U., Small, E. E., and Solomon, A. M.: Simulated influences of Lake Agassiz on the climate of central North America 11 000 years ago, *Nature*, 405, 334–337, 2000.
- Jones, M. C. and Yu, Z.: Rapid deglacial and early Holocene expansion of peatlands in Alaska, *P. Natl. Acad. Sci. USA*, 107, 7347–7352, 2010.
- Joussaume, S., Taylor, K. E., Braconnot, P., Mitchell, J., Kutzbach, J. E., Harrison, S. P., Prentice, I. C., Broccoli, A. J., Abe-Ouchi, A., Bartlein, P. J., Bonfils, C., Dong, B., Guiot, J., Herterich, K., Hewitt, C. D., Jolly, D., Kim, J. W., Kislov, A., Kitoh, A., Loutre, M. F., Masson, V., McAvaney, B., McFarlane, N., de Noblet, N., Peltier, W. R., Peterschmitt, J. Y., Pollard, D., Rind, D., Royer, J. F., Schlesinger, M. E., Syktus, J., Thompson, S. L., Valdes, P., Vettoretti, G., Webb, R. S., and Wyputta, U.: Monsoon changes for 6000 years ago: results of 18 simulations from the Paleoclimate Modeling Intercomparison Project (PMIP), *Geophys. Res. Lett.*, 26, 859–862, 1999.
- Kaufman, D. S., Ager, T. A., Anderson, N. J., Anderson, P. M., Andrews, J. T., Bartlein, P. J., Brubaker, L. B., Coats, L. L., Cwynar, L. C., Duvall, M. L., Dyke, A. S., Edwards, M. E., Eisner, W. R., Gajewski, K., Geirsdóttir, A., Hu, F. S., Jennings, A. E., Kaplan, M. R., Kerwin, M. W., Lozhkin, A. V., MacDonald, G. M., Miller, G. H., Mock, C. J., Oswald, W. W., Otto-Bliesner, B. L., Porinchu, D. F., Ruhland, K., Smol, J. P., Steig, E. J., and Wolfe, B. B.: Holocene thermal maximum in the western Arctic (0–180° W), *Quaternary Sci. Rev.*, 23, 529–560, 2004.
- Keigwin, L. D., Donnelly, J. P., Cook, M. S., Driscoll, N. W., and Brigham-Grette, J.: Rapid sea-level rise and Holocene climate in the Chukchi Sea, *Geology*, 34, 861–864, 2006.
- Kokorowski, H. D., Anderson, P. M., Mock, C. J., and Lozhkin, A. V.: A re-evaluation and spatial analysis of evidence for a Younger Dryas climatic reversal in Beringia, *Quaternary Sci. Rev.*, 27, 1710–1722, 2008.
- Kutzbach, J. E. and Gallimore, R. G.: Sensitivity of a coupled atmosphere mixed layer ocean model to changes in orbital forcing at 9000 years BP, *J. Geophys. Res.-Atmos.*, 93, 803–821, 1988.
- Liess, S., Snyder, P. K., and Harding, K. J.: The effects of boreal forest expansion on the summer Arctic frontal zone, *Clim. Dynam.*, 38, 1805–1827, doi:10.1007/s00382-011-1064-7, 2012.
- Lozhkin, A. V., Anderson, P. M., Eisner, W. R., Ravako, L. G., Hopkins, D. M., Brubaker, L. B., Colinvaux, P. A., and Miller, M. C.: Late Quaternary lacustrine pollen records from southwestern Beringia, *Quaternary Res.*, 39, 314–324, 1993.
- Lozhkin, A. V., Anderson, P., Eisner, W. R., and Solomatkina, T. B.: Late glacial and Holocene landscapes of central Beringia, *Quaternary Res.*, 76, 383–392, 2011.
- Lynch, A. H., Bonan, G. B., Chapin III, F. S., and Wu, W.: Impact of tundra ecosystems on the surface energy budget and climate of Alaska, *J. Geophys. Res.-Atmos.*, 104, 6647–6660, 1999.
- Lynch, A. H., Slater, A. G., and Serreze, M.: The Alaskan Arctic frontal zone: forcing by orography, coastal contrast, and the boreal forest, *J. Climate*, 14, 4351–4362, 2001.
- Lynch, A. H., Rivers, A. R., and Bartlein, P. J.: An assessment of the influence of land cover uncertainties on the simulation of global climate in the early Holocene, *Clim. Dynam.*, 21, 243–256, 2003.
- MacDonald, G. M., Beilman, D. W., Kremenetski, K. V., Sheng, Y., Smith, L. C., and Velichko, A. A.: Rapid early development of circumarctic peatlands and atmospheric CH₄ and CO₂ variations, *Science*, 214, 385–388, 2006.
- Manley, W. F.: Postglacial Flooding of the Bering Land Bridge: a Geospatial Animation: INSTAAR, University of Colorado, v1, available at: http://instaar.colorado.edu/QGISL/bering_land_bridge (last access: 12 May 2014), 2002.
- Mann, D. H., Reanier, R. E., Peteet, D. M., Kunz, M. L., and Johnson, M.: Environmental change and Arctic Paleoindians, *Arctic Anthropol.*, 38, 119–138, 2001.
- McGuire, A. D., Ruess, R. W., Lloyd, A., Yarie, J., Clein, J. S., and Juday, G. P.: Vulnerability of white spruce tree growth in interior Alaska in response to climate variability: dendrochronological, demographic, and experimental perspectives, *Can. J. Forest Res.*, 40, 1197–1209, 2010.
- Mearns, L. O., Arritt, R., Biner, S., Bukovsky, M. S., McGinnis, S., Sain, S., Caya, D., Correia, J., Flory, D., Gutowski, W., Takle, E. S., Jones, R., Leung, R., Moufouma-Okia, W., McDaniel, L., Nunes, A. M. B., Qian, Y., Roads, J., Sloan, L., and Snyder, M.: The North American regional climate change assessment program: overview of phase I results, *B. Am. Meteorol. Soc.*, 93, 1337–1362, 2012.
- Miller, G. H., Brigham-Grette, J., Alley, R. B., Anderson, L., Bauch, H. A., Douglas, M. S. V., Edwards, M. E., Elias, S. A., Finney, B. P., Fitzpatrick, J. J., Funder, S. V., Herbert, T. D., Hinzman, L. D., Kaufmann, D. S., MacDonald, G. M., Polyak, L., Robock, A., Serreze, M. C., Smol, J. P., Spielhagen, R., White, J. W. C., Wolfe, A. P., and Wolff, E. W.: Temperature and precipitation history of the Arctic, *Quat. Sci. Rev.*, 29, 1679–1715, 2010.
- Mock, C. J., Bartlein, P. J., and Anderson, P. M.: Atmospheric circulation patterns and spatial climatic variations in Beringia, *Int. J. Climatol.*, 18, 1085–1104, 1998.
- Monnin, E., Indermuhle, A., Allenbach, A., Fluckiger, J., Stauffer, B., Stocker, T. F., Raynaud, D., and Barnola, J. M.: Atmospheric CO₂ concentrations over the last glacial termination, *Science*, 291, 112–114, 2001.
- Myers-Smith, I. H., Forbes, B. C., Wilmking, M., Hallinger, M., Lantz, T., Blok, D., Tape, K. D., Macias-Fauria, M., Sass-Klaassen, U., Lévesque, E., Boudreau, S., Ropars, P., Hermanutz, L., Trant, A., Collier, L. S., Weijers, S., Rozema, J., Rayback, S. A., Schmidt, N. M., Schaepman-Strub, G., Wipf, S., Rixen, C., Ménard, C. B., Venn, S., Goetz, S., Andreu-Hayles, L., Elmendorf, S., Ravolainen, V., Welker, J., Grogan, P., Epstein, H. E., and Hik, D. S.: Shrub expansion in tundra ecosystems: dynamics, impacts and research priorities, *Environ. Res. Lett.*, 6, 045509, doi:10.1088/1748-9326/6/4/045509, 2011.
- Oechel, W. C., Hastings, S. J., Vourlitis, G., Jenkins, M., Riechers, G., and Grulke, N.: Recent change of Arctic tundra ecosystems from a net carbon dioxide sink to a source, *Nature*, 361, 520–523, 1993.
- Oncley, S. P., Lenschow, D. H., Campos, T. L., Davis, K. J., and Mann, J.: Regional-scale surface flux observations across the boreal forest during BOREAS, *J. Geophys. Res.-Atmos.*, 102, 29147–29154, 1997.

- Osterkamp, T. E. and Romanovsky, V. E.: Evidence for warming and thawing of discontinuous permafrost in Alaska, *Permafrost Periglac.*, 10, 17–37, 1999.
- Pal, J. S., Giorgi, F., Bi, X., Elguindi, N., Solon, F., Gao, X., Rausher, S. A., Francisco, R., Zakey, A., Winter, J., Ashfaq, M., Syed, F. S., Bell, J. L., Diffenbaugh, N. S., Karmacharya, J., Konaré, A., Martínez, D., Da Rocha, R. P., Sloan, L. C., and Steiner, A. L.: Regional climate modeling for the developing world: the ICTP RegCM3 and RegCNET, *B. Am. Meteorol. Soc.*, 88, 1395–1409, doi:10.1175/BAMS-88-9-1395, 2007.
- Peltier, W. R.: Ice age paleotopography, *Science*, 265, 195–201, 1994.
- Pielke, R. A. and Vidale, P. L.: The boreal forest and the polar front, *J. Geophys. Res.-Atmos.*, 100, 25755–25758, doi:10.1029/95JD02418, 1995.
- Pinot, S., Ramstein, G., Harrison, S. P., Prentice, I. C., Guiot, J., Stute, M., and Joussaume, S.: Tropical paleoclimates at the Last Glacial Maximum: comparison of Paleoclimate Modeling Intercomparison Project (PMIP) simulations and paleodata, *Clim. Dynam.*, 15, 857–874, 1999.
- Pollard, D. and Thompson, S. L.: Climate and ice-sheet mass balance at the last glacial maximum from the GENESIS version 2 global climate model, *Quaternary Sci. Rev.*, 16, 841–863, 1997.
- Prentice, I. C. and Webb, T.: BIOME 6000: reconstructing global mid-Holocene vegetation patterns from palaeoecological records, *J. Biogeogr.*, 25, 997–1005, 1998.
- Prentice, I. C., Jolly, D., and BIOME 6000 Participants: Mid-Holocene and glacial-maximum vegetation geography of the northern continents and Africa, *J. Biogeogr.*, 27, 507–519, 2000.
- Rekacewicz, P.: Circumpolar Active-Layer Permafrost System (CAPS), version 1.0, UNEP, available at: http://nsidc.org/cryosphere/frozensground/whereis_fg.html (last access: 12 May 2014), 1998.
- Ritchie, J. C. and Hare, F. K.: Late-Quaternary vegetation and climate near the arctic tree line of northwestern North America, *Quaternary Res.*, 1, 331–342, 1971.
- Ritchie, J. C., Cwynar, L. C., and Spear, R. W.: Evidence from northwest Canada for an early Holocene Milankovitch thermal maximum, *Nature*, 205, 126–128, 1983.
- Rivers, A. A. and Lynch, A. H.: On the influence of land cover on early Holocene climate in northern latitudes, *J. Geophys. Res.-Atmos.*, 109, D21114, doi:10.1029/2003JD004213, 2004.
- Romanovskii, N. N., Hubberten, H. W., Gavrillov, A. V., Tumskey, V. E., Tipenko, G. S., Grigoriev, M. N., and Siegert, C.: Thermokarst and land–ocean interactions, Laptev Sea Region, Russia, *Permafrost Periglac.*, 11, 137–152, 2000.
- Romanovsky, V. E., Smith, S. L., and Christiansen, H. H.: Permafrost thermal state in the polar Northern Hemisphere during the International Polar Year 2007–2009: a Synthesis, *Permafrost Periglac.*, 21, 106–116, 2010.
- Ruddiman, W. F., Vavrus, S. J., and Kutzbach, J. E.: A test of the overdue-glaciation hypothesis, *Quaternary Sci. Rev.*, 24, 1–10, doi:10.1016/j.quascirev.2004.07.010, 2005.
- Serreze, M. C., Holland, M. H., and Stroeve, J.: Perspectives on the Arctic's shrinking sea-ice cover, *Science*, 315, 1533–1536, doi:10.1126/science.1139426, 2007.
- Smith, L. C., Sheng, Y., MacDonald, G. M., and Hinzman, L. D.: Disappearing Arctic lakes, *Science*, 308, 1429, doi:10.1126/science.1108142, 2005.
- Smith, T. M. and Shugart, H. H.: The transient response of terrestrial carbon storage to a perturbed climate, *Nature*, 361, 523–526, 1993.
- Steinhauser, F.: Climatic Atlas of North And Central America, I, Maps of Mean Temperature and Precipitation, Hungary-World Meteorological Organization, UNESCO, 28 maps, 1979.
- Sturm, M., Racine, C., and Tape, K.: Climate change – increasing shrub abundance in the Arctic, *Nature*, 411, 546–547, 2001.
- Sturm, M., Douglas, T., Racine, C., and Liston, G. E.: Changing snow and shrub conditions affect albedo with global implications, *J. Geophys. Res.-Biogeo.*, 110, G01004, doi:10.1029/2005JG000013, 2005.
- Subin, Z. M., Murphy, L. N., Li, F., Bonfils, C., and Riley, W. J.: Boreal lakes moderate seasonal and diurnal temperature variation and perturb atmospheric circulation: analyses in the Community Earth System Model 1 (CESM1), *Tellus*, 64, 15639, doi:10.3402/tellusa.v64i0.15639, 2012.
- Swann, A. L., Fung, I. Y., Levis, S., Bonan, G. B., and Doney, S. C.: Changes in Arctic vegetation amplify high-latitude warming through the greenhouse effect, *P. Natl. Acad. Sci. USA*, 107, 1295–1300, 2010.
- Tabor, C. R., Poulsen, C. J., and Pollard, D.: Mending Milankovitch's theory: obliquity amplification by surface feedbacks, *Clim. Past*, 10, 41–50, doi:10.5194/cp-10-41-2014, 2014.
- TEMPO Members: Potential role of vegetation feedback in the climate sensitivity of high-latitude regions: a case study at 6000 years B.P., *Global Biogeochem. Cy.*, 10, 727–736, 1996.
- Thomas, G. and Rowntree, P. R.: The boreal forests and climate, *Q. J. Roy. Meteor. Soc.*, 118, 469–497, 1992.
- Thompson, S. L. and Pollard, D.: A global climate model (GENESIS) with a land-surface transfer scheme (LSX). Part I: Present climate simulation, *J. Climate*, 8, 732–761, doi:10.1175/1520-0442(1995)008<0732:AGCMWA>2.0.CO;2, 1995.
- Timm, O., Timmermann, A., Abe-Ouchi, A., Saito, F., and Segawa, T.: On the definition of seasons in paleoclimate simulations with orbital forcing, *Paleoceanography*, 23, PA2221, doi:10.1029/2007PA001461, 2008.
- Walsh, J. E., Zhou, X., Portis, D., and Serreze, M. C.: Atmospheric contribution to hydrologic variations in the Arctic, *Atmos. Ocean*, 32, 733–755, 1994.
- Walter, K. M., Zimov, S., Chanton, J. P., Verbyla, D., and Chapin, F. S.: Methane bubbling from Siberian thaw lakes as a positive feedback to climate warming, *Nature*, 443, 71–75, 2006.
- Walter, K. M., Edwards, M. E., Grosse, G., Zimov, S. A., and Chapin III, F. S.: Thermokarst lakes as a source of atmospheric CH₄ during the last deglaciation, *Science*, 318, 633–636, 2007.
- Walter Anthony, K. M., Zimov, S. A., Grosse, G., Jones, M. C., Anthony, P. M., Chapin III, F. S., Finlay, J. C., Mack, M. C., Davydov, S., Frenzel, P., and Frohking, S.: A shift of thermokarst lakes from carbon sources to sinks during the Holocene epoch, *Nature*, 511, 452–456, 2014.
- Williams, J. R. and Yeend, W. E.: Deep thaw lake basins in the inner Arctic Coastal Plain, Alaska, in: U. S. Geological Survey in Alaska: Accomplishments During 1978, edited by: Johnson, K. M. and Williams, J. R., USGS Circular, 804-B, B35–B37, 1979.
- World Meteorological Organization: Climatic Atlas of Asia, WMO-Unesco-Goscomgidromet, Geneva, Switzerland, 1981.

Yokoyama, Y., Lambeck, K., De Deckker, P., Johnston, P., and Field, L. K.: Timing of the Last Glacial Maximum from observed sea-level minima, *Nature*, 406, 713–716, 2000.

Zimov, S. A., Schuur, E. A. G., and Chapin III, F. S.: Permafrost and the global carbon budget, *Science*, 312, 1612–1613, 2006.